THESIS FOR THE DEGREE OF DOCTOR OF PHILOSOPHY IN SOLID AND STRUCTURAL MECHANICS

Digital twins for rail damage evolution in railway curves

Field data, model calibration and reduced order models

CAROLINE ANSIN

Department of Industrial and Materials Science
Division of Material and Computational Mechanics
CHALMERS UNIVERSITY OF TECHNOLOGY

Göteborg, Sweden 2025

Digital twins for rail damage evolution in railway curves
Field data, model calibration and reduced order models
CAROLINE ANSIN
ISBN 978-91-8103-320-5

Doktorsavhandlingar vid Chalmers tekniska högskola
Ny serie nr. 5777
ISSN 0346-718X

Department of Industrial and Materials Science
Division of Material and Computational Mechanics
Chalmers University of Technology
SE-412 96 Göteborg
Sweden
Telephone: +46 (0)31-772 1000

Cover:
Illustration of digital twin framework, the numerical model (right) is continuously updated by field measurements (left). The numerical model can then forecast material damage in the railhead.

Chalmers Reproservice
Göteborg, Sweden 2025

Digital twins for rail damage evolution in railway curves
Field data, model calibration and reduced order models

CAROLINE ANSIN
Department of Industrial and Materials Science
Division of Material and Computational Mechanics
Chalmers University of Technology

Abstract

Rails in railway tracks are subjected to complex rolling-sliding contact conditions that can cause surface and subsurface damage in the form of wear, plastic deformation, and Rolling Contact Fatigue (RCF). The prevailing operational conditions and maintenance practices of the rails strongly influence the evolution of this damage. If not managed properly, these mechanisms can degrade vehicle steering performance, increase noise and vibration levels, and in severe cases lead to rail failure or derailment. However, maintenance is costly and is difficult to plan correctly. Therefore, the ability to predict damage evolution is essential for effective maintenance planning and extending the rails' service life.

This thesis presents a digital twin framework for the long-term prediction of rail damage evolution in railway curves under operational traffic conditions. The framework integrates field measurements of rail profiles with numerical simulations using models for the mechanical behavior of the rails. This enables continuous calibration and updating of model parameters based on observed rail behavior. The simulations are performed using models of dynamic vehicle-track interactions and accumulative rail damage computations considering plastic deformation, wear, and surface RCF. The calibration process adjusts parameters related to vehicle, track, contact model, and material properties, such as wear coefficients or yield limits, to ensure that the simulated degradation mimics the field-measured rail profile evolution. After calibration, the digital twins can predict railhead damage more accurately.

To speed up numerical efficiency, a reduced order modeling framework has been developed for 3D rail geometry and plastic deformations. The framework adopts a convective coordinate system that follows a moving contact load and assumes a steady-state response. This transforms the transient moving contact problem into a stationary formulation, where the material history is tracked along streamlines in the spatial mesh. An iterative scheme couples the displacement and plastic strain fields. In addition, the Proper Generalized Decomposition (PGD) has been adopted to provide an efficient representation of the 3D displacement field through domain decomposition and parametrization of the contact loads. The framework achieves accuracy comparable to that of a full 3D finite-element analysis at a fraction of the cost.

The resulting digital twins efficiently and accurately forecast profile geometry changes of railheads in curved tracks. Thus, this work demonstrates the feasibility of using digital twins to predict rail damage evolution and provides a step towards building a foundation for data-informed maintenance planning.

Keywords: digital twin, railway curves, plasticity, wear, Rolling Contact Fatigue (RCF), Proper Generalized Decomposition (PGD), Reduced Order Modeling (ROM), Steady-state in rolling contact, dynamic vehicle-track interaction

To Love

Preface

This work was carried out at the Department of Industrial and Materials Science at Chalmers University of Technology between December 2020 and November 2025. The research project MU40 "Digital Twin of Reprofiled Rails" is part of CHARMEC's (Chalmers Railway Mechanics, www.chalmers.se/charmec) center. Parts of the study were funded by the Horizon Europe research and innovation program in Europe Rail under In2Track2, In2Track3, and IAM4RAIL projects under grant agreements numbers 826255, 101012456, and 101101966, respectively. The author thanks the Swedish Transport Administration (Trafikverket) for their support. The numerical computations were enabled by resources provided by the National Academic Infrastructure for Supercomputing in Sweden (NAISS) at Chalmers Center for Computational Science and Engineering (C3SE), partially funded by the Swedish Research Council through grant agreement number 2022-06725.

Acknowledgements

This has been a long journey with a few sharp curves and some fatigue, but I have somehow managed to arrive at the right station. I owe that to the many people who have made these years both rewarding and fun.

First and foremost, my sincere gratitude goes to my supervisors, Professor Fredrik Larsson, Professor Magnus Ekh, Associate Professor Björn Pålsson, and Professor Ragnar Larsson, for your guidance, support, and patience throughout this research project. Although having four supervisors sometimes meant that my "to-do" list grew long, it has been a privilege to learn from your expertise and to engage in interesting discussions. A special thanks to Fredrik, you have made model order reduction look (somewhat) easy, and I have never met anyone who can dive into a problem as quickly as you do.

I would also like to acknowledge the CHARMEC research group and all our project partners. You have provided valuable input, engaging discussions, and helped me see the broader perspective of this research.

To my colleagues at Chalmers, I never expected to gain so many new friends. You are always ready to help when needed and make every day at work more enjoyable. My office mate, Gabriel, deserves a special mention for not only bringing my 3D models to life but also ensuring that our office stays seasonally decorated.

To my friends outside academia, thank you for reminding me that there is more to the world than railway tracks.

Primus, my cat and involuntary alarm clock, thank you for making sure I get out of bed every morning. You have been both a source of comfort and an expert in cat-astrophic ways of demanding attention.

To my family, thank you for your constant encouragement throughout my studies. Even after five years, my research still remains something of a mystery to you; perhaps this thesis will help.

Finally, to my dear husband, Love, for your kindness and support. You have endured countless dinner monologues about work (which, in truth, were probably closer related to gossip than research reflections). You have been there through every curve of this journey, keeping me on track all the way.

Gothenburg, October 2025
Caroline Ansin

Thesis

This thesis consists of an extended summary and the following appended papers:

Paper A C. Ansin, B. Pålsson, M. Ekh, F. Larsson and R. Larsson, "Simulation and field measurements of the long-term rail surface damage due to plasticity, wear and surface rolling contact fatigue cracks in a curve". *Proceedings of the 12th International Conference on Contact Mechanics and Wear of Rail/Wheel Systems (CM2022)*, Melbourne Australia, September 2022.

Paper B C. Ansin, B. Pålsson, "Influence of model parameters on the predicted rail profile wear distribution in a curve". *Internal Report, Chalmers University of Technology* (2023).

Paper C C. Ansin, M. Ekh, B. Pålsson, F. Larsson and R. Larsson, "Simulations and field measurements of long-term rail profile wear in curves". *Proceedings of the 13th International Conference on Contact Mechanics and Wear of Rail/Wheel Systems (CM2025)*, Tokyo, Australia, September 2022.

Paper D C. Ansin, F. Larsson and R. Larsson, "Fast simulation of 3D elastic response for wheel–rail contact loading using Proper Generalized Decomposition". *Computer Methods in Applied Mechanics and Engineering.* **417** (2023), 0045-7825, 116466. DOI: 10.1016/j.cma.2023.116466

Paper E C. Ansin, F. Larsson and R. Larsson, "Prediction of evolving plasticity in rails under steady state rolling contact based on Reduced-Order Modeling". *Computer Methods in Applied Mechanics and Engineering.* **438** (2025), 0045-7825, 117828. DOI: 10.1016/j.cma.2025.117828

The appended papers were collaboratively prepared with co-authors. The author of this thesis was responsible for the major part of the work and contributed as follows: took part in planning the papers and formulating the theory, developed the computational framework, performed numerical simulations, interpreted the results, and wrote major parts of the papers.

Contents

Part I
Extended Summary

1. Introduction

1.1 Background and motivation

Railway transportation is a safe and sustainable mode of transportation for both passengers and freight. In terms of passenger safety, Åkesson [1] estimated that rail travel was approximately one hundred times safer than car travel per passenger-kilometer traveled in Sweden between 1999 and 2008. Furthermore, it has been documented that rail transportation has a low carbon footprint. According to Doll et al. [2], it has the lowest CO_2 emissions per distance traveled and per tonne transported among all transport modes. Specifically, rail freight produces around one-tenth of the CO_2 emissions per tonne transported compared to inland road freight. These advantages position rail transportation as a crucial element in the pursuit of sustainable mobility and in achieving national and international climate goals. With these benefits comes a continually growing demand for rail transportation, a trend that is expected to persist for the next two to three decades [3]. However, the expansion of available track infrastructure has not kept pace with the increasing volume of transportation. At the same time, higher operating speeds and increased axle loads have placed additional stress on the railway network. This has led to an increase in rail degradation, resulting in a corresponding need for increased maintenance. As a result, maintenance costs have risen, and operational disturbances have become more frequent in recent years.

Rail degradation results from repeated wheel–rail interactions and involves several damage mechanisms, including wear, plastic deformation, and Rolling Contact Fatigue (RCF). Over time, with many wheel passages, these mechanisms can lead to alterations in the rail geometry and can result in the initiation and propagation of surface (or subsurface) cracks. These damage mechanisms can also interact. When contact tractions generate stresses that exceed the material's yield limit, inelastic deformation accumulates, and residual stresses develop within the contact region [4]. As the loading process continues, plastic strains can accumulate, which can promote RCF crack initiation [5]. It can also result in a work-hardened rail material near the contact surface, which influences both wear resistance and crack growth behavior [4, 6]. Meanwhile, wear can remove the work-hardened material as well as remove surface RCF cracks completely or reduce their length [7].

In curved track sections, high tangential contact forces and creepages govern these damage mechanisms and their interactions. In tight curves, wear tends to dominate and may remove RCF cracks. In shallower curves, lower wear rates allow RCF cracks to develop and propagate more easily. If such degradation is not properly managed, it can lead to changes in rail geometry and crack propagation, which reduce steering performance, increase noise and vibration, and, in severe cases, result in rail failure or

derailment.

To mitigate rail damage and extend the rails' service life, regular maintenance and inspections are necessary. These activities are also critical to minimize service disruptions, ensure operational safety, and control costs. In Sweden, for instance, approximately 40 % of the total maintenance costs of tracks are associated with wear and damage related to RCF [8]. Furthermore, the Swedish Transport Administration reported that track maintenance cost was about 2.4 billion SEK in 2016 [9]. Such numbers underline the economic importance of maintenance optimization. A variety of techniques are used to manage surface damage and restore desired rail profiles. Common techniques used in this process are grinding, milling, rail replacement, and preventative measures such as lubrication. Grinding is the most widely applied method for reprofiling the rail to remove surface irregularities and prevent crack initiation and propagation.

This maintenance action can be either corrective or preventive [10]. In corrective grinding, material removal is performed only after visible damage has occurred. This method typically requires more material removal and multiple grinding passes. Preventive grinding is conducted at fixed intervals. It can be performed before the development of visible defects, using smaller material removal depths. Although preventive strategies generally result in better long-term rail conditions and lower total costs [11], they also require accurate forecasts of rail degradation to determine optimal grinding intervals. Thus, a challenge lies in finding a balance between extending the rails' service life, minimizing costs, and reducing traffic interruptions.

To support maintenance planning and improve the understanding of the governing damage mechanisms under different operational conditions, numerical models have been developed to simulate rail degradation and its evolution over time. Johansson et al. [12] and Skrypnyk et al. [13] investigated long-term crossing degradation by coupling multibody dynamics (MBD) vehicle–track simulations with models for accumulated wear and plastic deformation. These models account for varying traffic conditions. Hossein-Nia et al.[14] applied a similar approach to wheels, focusing on wear and RCF. Krishna et al. [15] extended such modeling to curved track sections, predicting wear, RCF evolution, and maintenance needs for rails of different curve radii and traffic scenarios. More detailed analysis was conducted by Trummer et al. [16], who modeled RCF crack initiation on wheels and rails by accounting for severe plastic shear deformation. Additionally, Vo et al. [17] examined individual contact scenarios using a detailed 3D elastic–plastic Finite Element (FE) model that captures material ratcheting, wear, and surface-initiated RCF cracks.

While these studies have advanced the understanding of rail degradation, most are limited to short-term analyses, simplified assumptions, or consideration of only one or a few damage mechanisms. These simplifications and omissions are often necessary because high-fidelity numerical models, such as FE models, are computationally intensive and therefore impractical for long-term simulations. Consequently, existing simulation techniques have limited predictive capability for extended operational periods or for cases involving multiple damage mechanisms. Moreover, few studies validate numerical results against field measurements, which partly explains why numerical simulations are rarely used for maintenance planning in practice.

Therefore, there is a need for computationally efficient and data-informed models

that can accurately predict long-term rail damage under realistic traffic conditions. One promising approach to achieving this is using digital twins. A digital twin can be defined as a virtual representation of a physical system that mirrors its behavior through continuous data exchange between the physical and virtual counterparts [18, 19]. The virtual model is updated using measurement data from the physical system and, in turn, performs simulations to predict its current or future states. In this thesis, the simulations predict the long-term evolution of rail damage. Thereby, the digital twin can support decision tools for more effective maintenance planning.

However, implementing digital twins to predict long-term rail damage presents its own challenges. The simulations must be both accurate and computationally efficient to allow for long-term forecasts. For many applications, such as the one considered in this thesis, accurate predictions are retained through nonlinear transient FE simulations in full 3D, resulting in long computational times. To overcome this, Reduced-Order Modeling (ROM) [20–23] can be used to construct low-dimensional approximations of full-order models. A ROM reduces the computational complexity of high-dimensional, multiphysics, or parametric problems while maintaining sufficient accuracy. One ROM approach is the Proper Generalized Decomposition (PGD) method [22], an *a priori* technique that constructs the reduced representation of the solution directly during the computation process. In PGD, the solution is expressed as a finite sum of separable functions, each depending on a subset of the problem coordinates.

1.2 Research objectives

The overall goal of the research in this thesis is to *develop digital twins that are computationally efficient and can predict long-term rail damage in curved railway sections under operational traffic*. By integrating numerical simulations with field measurements, the proposed framework aims to provide reliable forecasts of rail damage evolution while maintaining fast and memory-efficient simulations by using tools such as ROMs. Ultimately, the digital twins are intended to serve as decision-support tools to optimize maintenance strategies, such as rail grinding or replacement.

To accomplish this objective, the specific sub-goals can be summarized as:

- Develop and calibrate a numerical model for use in a digital twin framework, capable of simulating the evolution of railhead geometry and damage under relevant operational traffic conditions.
  - This process involves parameter calibration (e.g., wear rates, yield limits, vehicle, and track parameters), using field measurements, as well as refinement of contact modeling. The predictive performance is validated against independent field data.

- Improve the numerical efficiency of simulation tools to facilitate rapid predictions.
  - This involves reducing the cost of 3D FE analysis by using the PGD method for rail sections.

1.3 Scope and limitations

In this thesis, each digital twin is defined as a numerical model representing a single high (outer) railhead cross-section (see Figure 1.1). The analyses focus solely on the high rail in curves, where surface damage is most pronounced. The model is continuously updated using cross-sectional rail geometry field measurements to improve the accuracy of the predictions. The numerical model predicts long-term changes of the railhead geometry, accounting for surface wear and plastic deformation. The model also predicts the risk of RCF crack initiation, although no such measurement data are available for either calibration or validation. Moreover, the coupling between the damage mechanisms is limited in the simulations, and the subsequent crack propagation has not been modeled.

Vehicle-track dynamic simulations are carried out for a representative load-collective that captures the variability of operational traffic conditions. These analyses rely on existing contact models implemented either in the MBD software or through the Hertzian-inspired metamodel proposed by Skrypnyk et al. [24]. In all cases, the wheel is assumed to behave linearly elastic, while the rail is modeled as either linear elastic or, to some extent, inelastic. However, the latter representation is simplified, particularly regarding the tangential contact behavior.

For the simulation of plastic deformation, FE models with cyclic plasticity are employed to capture the accumulation of inelastic strains in the railhead. The rail material is represented as an isotropic, elasto-plastic material at the macroscopic scale in a small-strain setting. Two modeling approaches are considered for the FE models, either simplified 2D FE analyses under plane-strain conditions, or the ROM framework developed in this thesis. The ROM is developed as a building block in the numerical model, analyzing the inelastic railhead deformation for known wheel loads. Its accuracy and efficiency are assessed by comparison with state-of-the-art 3D FE simulations.

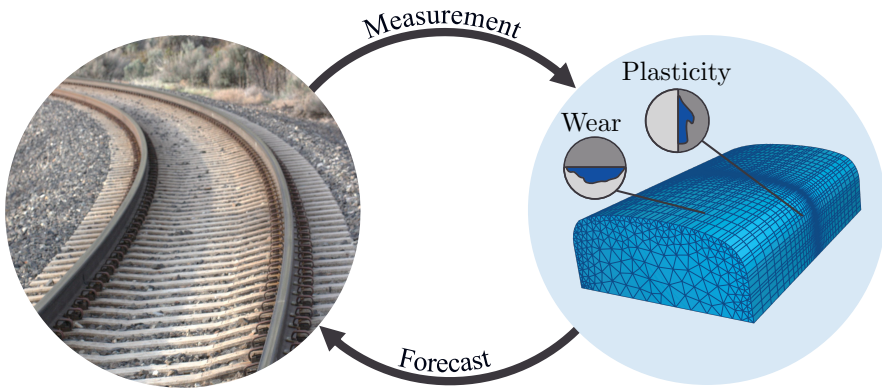

Figure 1.1: *Illustration of the digital twin approach for predicting rail damage. Field measurements from a physical rail (left) are used to update the numerical model of the railhead cross-section (right), which in turn forecasts future rail damage.*

2. Operational conditions for curved tracks

This chapter describes operational conditions and their influence on rail surface damage mechanisms resulting from wheel–rail contact. It also outlines the damage mechanisms considered in this work and provides an overview of the field measurement techniques used to evaluate rail conditions and monitor profile evolution.

2.1 Wheel–rail contact conditions

Damage to rails originates from the stresses and sliding motions generated at the wheel–rail interface. This interface is characterized by a small contact patch where heavy loads are transmitted. Typically, the area is around 1 to 2 cm^2 [25] with normal contact pressures reaching up to 1.5 GPa [26].

In addition to the normal problem described above, tangential stresses arise whenever the wheelset does not exhibit pure rolling along the rail. This causes slip within the contact patch. In practice, pure rolling is rarely achieved, since braking, acceleration, and the non-radial alignment of wheelsets in curves all generate relative motion in the contact patch, referred to as *creepage*.

When creepage occurs, Carter [27] and Fromm [28] showed that tangential tractions are not uniformly distributed across the contact area. Instead, the patch is divided into two zones as illustrated in Figure 2.1. A *stick region* at the leading edge, where wheel and rail surfaces adhere, and a *slip region* at the trailing edge, where relative sliding between wheel and rail takes place. The distribution of stick and slip areas, as well as the magnitude of the resulting tangential forces developed in the contact, depends on the applied creepage. As creepage increases, the slip portion of the contact area expands until full slip is reached. At full slip, the creep force is limited by Coulomb's friction law, that is, normal force multiplied by the coefficient of friction.

The location of the contact point between the wheel and the rail is determined by the geometry of the profiles and their relative position. On a straight track, contact generally occurs between the wheel tread and top of the rail. However, on a curved track, the lateral displacement of the wheelset shifts the contact point toward the gauge corner on the high rail. This can result in a secondary contact between the wheel flange and the rail gauge corner, as illustrated in Figure 2.2. Multiple contact points may also occur due to irregularities in the wheel and rail profiles.

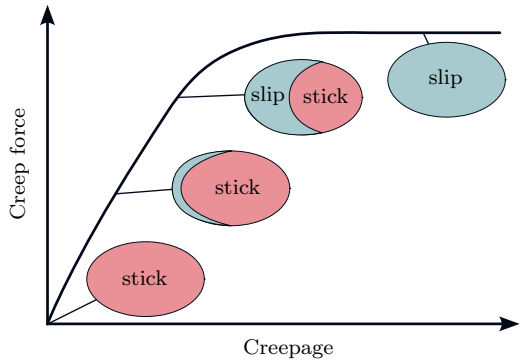

Figure 2.1: *Evolution of stick and slip regions within the contact area for increasing creepage.*

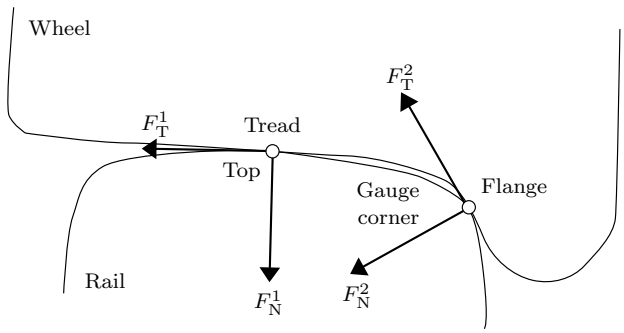

Figure 2.2: *The two-point contact between the wheel and rail results in normal F_{N} and tangential F_{T} loads on the rail at each point of contact.*

2.2 Operational conditions

Operational conditions determine the conditions in the wheel–rail contact and, consequently, contact positions, stresses, and damage mechanisms that develop over time. Key influencing factors include traffic loading, curve radius, wheel and rail geometries, and environmental conditions.

The characteristics of the traffic loading are central since variations in axle load, train length, and traffic mix (e.g., passenger versus freight vehicles) result in different load magnitudes, creepages, and number of overrollings. Higher axle loads increase the severity of the contact stress, and the number of wheel passages determines the cumulative damage. Vehicle speeds also affect the contact since higher speeds increase dynamic force amplitudes and alter the distribution of wheel–rail contact stresses along the rail. Additional influences arise from vehicle features such as tilting mechanisms and suspension systems, which modify the effective lateral acceleration and, consequently, the rail loading.

Track-related factors are equally important. The curve radius, cant, rail profile, and

track irregularities, together with the vehicle dynamics, determine how the wheelsets are positioned on and load the rail. In curves, steering of the wheelsets introduces creep forces, which increase as the radius of the curve decreases. Deviations or irregularities in track geometry modify wheel–rail contact positions and may cause transient variations in the normal and tangential contact forces. Variations in track stiffness, arising from differences in ballast condition, sleeper spacing, or rail pad stiffness, affect how loads are transmitted to the substructure and can amplify dynamic responses.

Environmental conditions also influence the wheel–rail contact and rail damage. Surface contaminants such as water, ice, or leaf layers alter the coefficient of friction [29]. This affects the balance between adhesion and slip in the contact and influences whether wear or RCF dominates. Dry, cold air in combination with snow trapped in the contact can promote the initiation of small cracks by lubricating crack faces and facilitating their growth [30]. Low temperatures in continuously welded rails generate tensile stresses that promote long crack growth and rail breaks. In contrast, high temperatures increase the risk of thermal buckling.

2.3 Rail surface damage mechanisms

Repeated wheel passages create complex combinations of normal and tangential shear loads, which impose high contact stresses on the railhead. This results in a multiaxial, cyclic stress state in the rail material involving compression and shear [31]. Over time, these loads lead to wear, plastic deformation, and crack formation due to RCF. Together, these damage mechanisms govern the deterioration of the rail surface, as illustrated in Figure 2.3.

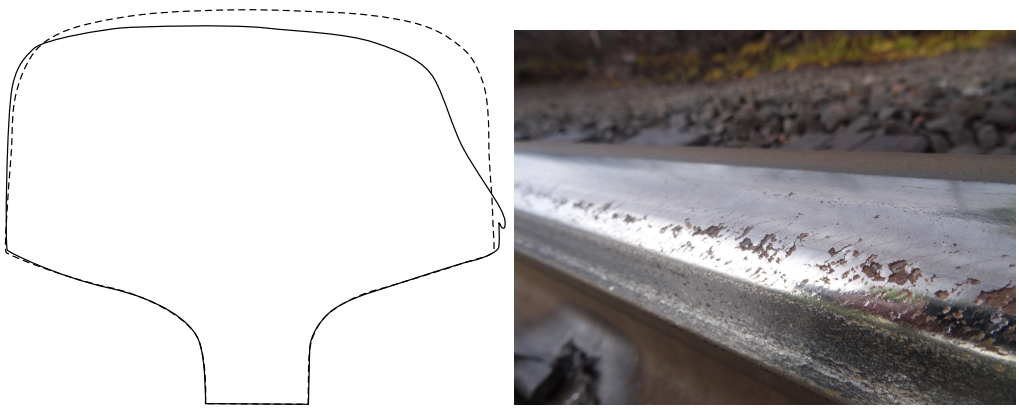

(a) *(b)*

Figure 2.3: *(a) nominal (BV50) and worn and deformed rail profile from [32], and (b) gauge corner RCF cracks, (head checks). Picture (right) from Anders Ekberg.*

Wear is the gradual removal of material from the contact surface due to slip within the contact patch. Depending on the contact conditions (e.g., sliding velocity and contact

pressure), the material properties of the contacting surfaces, and the presence of debris or contaminants, wear can range from mild to severe to catastrophic [33]. Mechanisms that can affect wear include oxidation, adhesion, abrasion, and fatigue [34]. Wear is most pronounced in tight curves, where large creepage and high tangential forces concentrate at the gauge corner of the high rail due to the combination of rolling and sliding contact (see Figure 2.3a). In agreement with this, Olofsson et al. [35] reported that the wear rate at the gauge corner can be up to ten times higher than at the rail top. While excessive wear shortens rail service life, increases the risk of derailment, and influences the dynamic behavior of the train, a moderate wear rate, referred to as the magic wear rate, can be beneficial since it optimally manages RCF by removing small cracks before they propagate [36].

Plastic deformation occurs near the surface where contact stresses locally exceed the yield strength of the rail steel. The plastically deformed material may flow laterally to the field side or create a lip beneath the gauge corner of the high rail [32, 35] as shown in Figure 2.3a. With repeated load cycles, plastic strain accumulates, known as *ratcheting*, and residual stresses develop [4]. This process leads to *cyclic hardening (or softening)* and a progressive change in the microstructure, resulting in a changed hardness and yield strength close to the surface. During such cyclic loading, the *Bauschinger effect* may occur, whereby prior plastic deformation reduces the yield strength in the reverse loading direction. Work-hardened material may resist further plastic flow, resulting in *plastic shakedown* and wear, as well as the tendency for crack initiation [4, 6]. Plastic deformation also introduces anisotropy in the near-surface layer due to the formation of texture and directional grain elongation [6, 37, 38]. As Larijani et al. [39] demonstrated, this anisotropy influences crack initiation and growth paths in the railhead.

RCF is closely related to plastic deformation. It develops under repeated loading, where cyclic compressive and shear stresses act on the surface layer and cause ratcheting when the ductility of the material is exceeded [5]. The resulting cracks may initiate at either the *surface* or the *subsurface* [31]. Surface-initiated RCF cracks are often referred to as head checks, gauge corner cracking, or squats. These cracks typically propagate at shallow angles into the rail surface and may lead to spalling, which is when portions of the surface material detach (cf. Figure 2.3b). This is also where wear and RCF are related, since the detachment of material from the surface can also be defined as wear [40]. If the crack propagates downward, it can cause transverse failure, which may potentially lead to a rail breakage and may cause derailment. The development of cracks due to RCF is a dominant damage mechanism for shallower curves, where the cracks are not removed by wear.

2.4 Field rail measurement techniques

Periodic maintenance inspections are used to monitor the condition of the rails and to detect potential issues before serious defects develop. These measurements allow for the identification of wear and plastic deformation and the detection of cracks. Various non-destructive methods are used to assess rail damage, including profile geometry changes and cracks. Rail profiles can be measured using vehicles equipped with laser sensors or using

a handheld device such as the MiniProf (rail instrument from Greenwood Engineering) [41]. The results can be used to quantify wear, plastic deformation, or material removed from grinding or milling. Cracks and subsurface defects, on the other hand, are detected using images, eddy-current, or ultrasonic techniques.

In this work, the Swedish Transport Administration provided MiniProf measurements of rail profiles in the field. Crack detection was not included in the test campaign. The data consists of rail profiles measured approximately every 60 meters along three curves every six months, beginning in May 2021. Between each measurement, roughly 10 Million Gross Tonnes (MGT) of traffic have passed on the tracks. The profiles were aligned at the field side relative to the initial (reference) measurement using the MiniProf Envision software [42] as illustrated in Figure 2.4b.

The rail profile data allows several indicators of material degradation to be evaluated. Examples of these indicators are shown in Figure 2.4 and have been described in more detail in **Paper A** and **Paper C**. Profile evolution (see Figure 2.4b) can be analyzed by computing changes of the geometry in the normal direction relative to the initial measurement. This highlights the development of distinct contact bands along the railhead. The total material removal caused by wear or grinding can be quantified by the reduced area a_{rd} (cf. Figure 2.4a), defined as the difference in area between the initial and measured profiles. Localized shape changes indicate plastic flow, which can be estimated using the isochoric shape change area a_{iso} (see Figure 2.4c), representing the volume-conserving deformation of the railhead. Plastic deformation in metals is generally isochoric, with only small elastic volume changes associated with residual stresses. Additionally, wear metrics of vertical h and horizontal s wear (cf. Figure 2.4a), measured at predefined positions on the profile, provide additional information on wear and grinding [43].

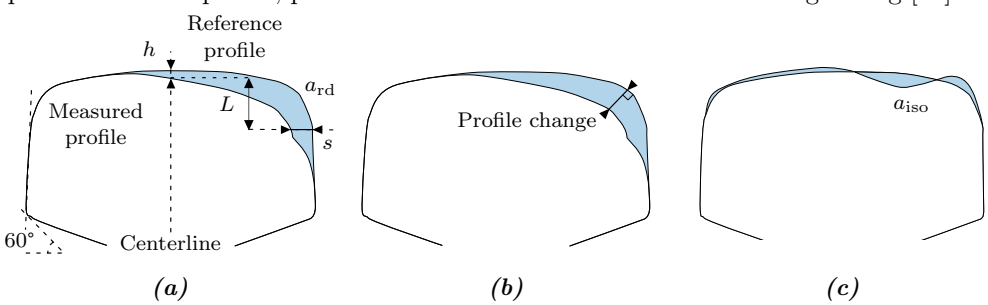

Figure 2.4: *Indicators of material degradation. (a) Rail profile alignment and wear metrics a_{rd}, h, and s, which are the reduced area, vertical, and horizontal wear, respectively. (b) Profile change measured in the normal direction relative to the reference profile. (b) Isochoric shape change area a_{iso} is the volume-conserving deformation indicating plastic flow.*

Figure 2.5 presents the measured rail profile data at the midpoint of a 996 m radius curve, which data is presented in more detail in **Paper C**. Figure 2.5a shows the profile change in the normal direction relative to the initial measurement. Figure 2.5b displays the progressive changes in the rail profile over time. The reduction in z-values with subsequent measurement dates indicates material loss. Figure 2.5b shows that the most

pronounced profile changes occur near $y = 0$ mm and $y = 25$ mm, which corresponds to contact bands at the top of the rail and the gauge corner, respectively. Larger changes on the field side (negative y) typically correspond to material removal by grinding rather than wear. Furthermore, Figure 2.6 displays the profile change for three different cross-sections after 10 MGT (211117) and 20 MGT (220512), where cross-section 2 is the same one as displayed in Figure 2.5. The figures show a variation in profile change between cross-sections for both traffic amounts, likely reflecting local differences in loading or measurement noise.

Although field measurements offer valuable insight, their accuracy is influenced by several factors. The results are sensitive to alignment errors between subsequent measurements, particularly when profile changes are small and similar in magnitude to the potential misalignment. The recorded grinding depths in the present work are only approximate because measurements were not taken immediately before and after grinding. This makes it difficult to distinguish between material removal due to grinding or wear. Moreover, the variations observed between cross-sections, as shown in Figure 2.6, may result from local differences in loading but could also reflect measurement uncertainty. These factors contribute to scatter in the data and limit the precision of quantitative model validation.

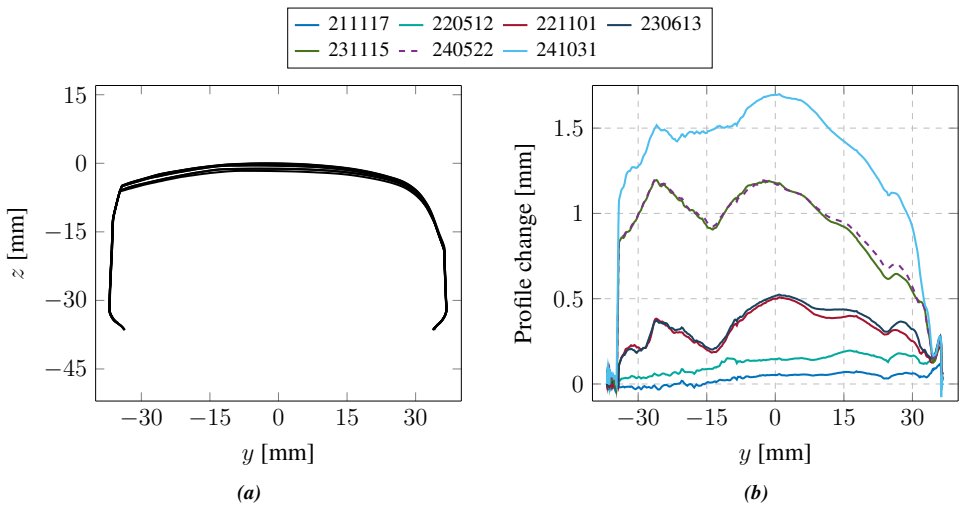

Figure 2.5: *Measured high rail profile cross-section at the midpoint of a 996 m radius curve. The gauge corner is to the right. (a) Rail profile development. (b) Profile change in the normal direction relative to the initial measurement.*

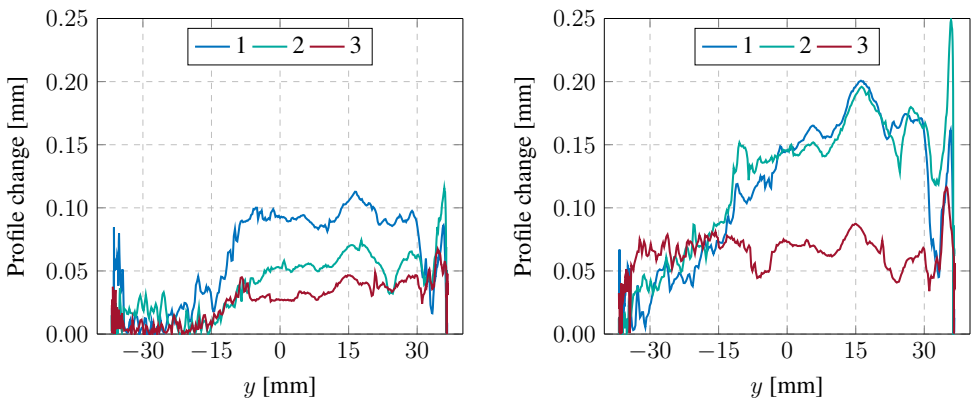

(a) *10 MGT* ***(b)*** *20 MGT*

Figure 2.6: *Measured profile change in the normal direction relative to the initial measurement for three different cross-sections (1,2,3) along a 996 m radius curve. The gauge corner is to the right, and the profile change is displayed after (a) 10 MGT, and (b) 20 MGT of traffic.*

3. Digital twin framework for rail damage evolution

This chapter presents a digital twin framework that is developed to evaluate long-term railhead damage in curved tracks. The numerical model combines vehicle-track dynamics with material degradation mechanisms and is calibrated using field measurements. The physical rails and measurement procedures supporting this calibration are described in Chapter 2.

3.1 Overview of digital twin framework

Digital twins provide computationally efficient, data-informed models capable of accurately predicting long-term railhead damage under realistic traffic conditions. Ultimately, such models aim to serve as decision-support tools for optimizing maintenance strategies, including rail grinding and replacement.

The digital twin links physical rails, represented by field measurements of railhead profiles, with a numerical model capable of simulating geometry changes of the railhead when it comes to surface wear and plastic deformation, as well as initiation of RCF cracks. Figure 3.1 illustrates the overall methodology.

The numerical model is based on a multidisciplinary simulation methodology presented in earlier work [12, 13, 44, 45], but has been further developed in this thesis to suit the present objectives. The simulations are applied in repeated cycles consisting of three steps (see Figure 3.1):

1. *Dynamic vehicle-track interaction* is simulated using MBD software to determine the wheel–rail contact positions, forces, and creepages for a given rail profile and a representative loading sequence.
2. *Rail damage evolution* is predicted based on the contact conditions, and considers accumulated wear, plastic deformation, and the initiation of RCF cracks.
3. *Rail profile update*, where the rail cross-section is modified to account for accumulated changes in wear and plastic deformation. The updated profile is then used in the next simulation cycle to get updated dynamic vehicle-track interactions.

By repeating these steps, the gradual evolution of the railhead profile can be simulated over long time periods. Since updating the railhead profile after every wheel pass would be computationally intensive, representative load sequences are generated and simulated to capture variations in traffic (e.g., wheel profiles, vehicle speeds, and axle loads). These load sequences are simulated a number of times before updating the dynamic loadings.

The framework operates as a digital twin by closing the loop between the physical and

numerical representations. Field measurements are used both to validate the numerical results and to calibrate model parameters to improve forecasts. This feedback process improves predictive accuracy and makes it possible to provide more reliable long-term forecasts of railhead damage than with an uncalibrated numerical model alone. The following sections provide a more detailed description of each step in the methodology and of the calibration procedure.

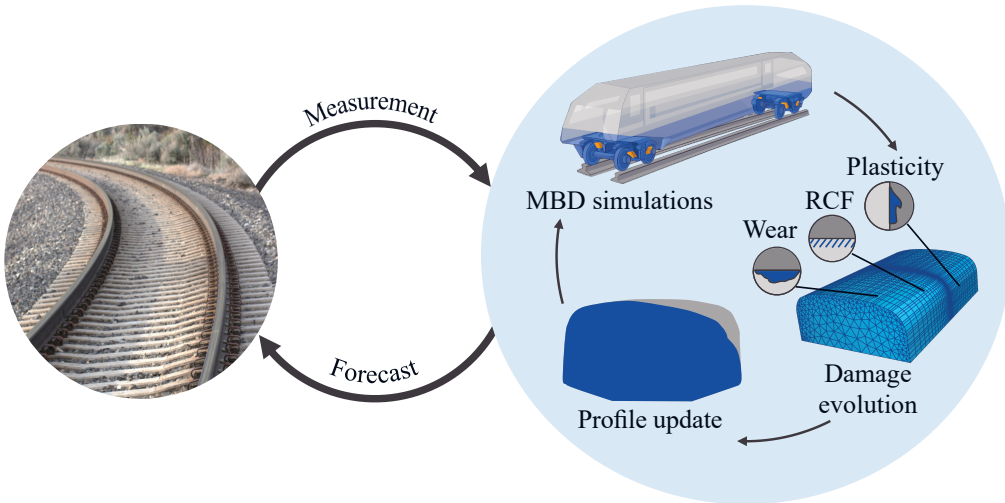

Figure 3.1: *Digital twin framework for predicting railhead surface damage. Field measurements of the railhead provide input to a numerical model that operates in repeated cycles of (1) dynamic vehicle-track interaction, (2) rail damage evolution (wear, plasticity, RCF initiation), and (3) rail profile updating. Model forecasts are validated and calibrated against measurements to improve long-term prediction accuracy.*

3.2 Dynamic vehicle-track interaction

To simulate dynamic vehicle-track interaction, MBD software is used. By solving the governing equations of motion, the MBD simulations capture how the vehicle (including car body, wheels, axles, etc.) interacts with the track under different traffic conditions. Such analyses are typically performed using commercial software packages such as GENSYS [46] or Simpack [47]. In this thesis, Simpack is used to generate load sequences for different traffic conditions in the time domain. The outputs provide information on the wheel–rail contact conditions, such as positions, contact areas, forces, and creepages, which are then used as input for subsequent calculations of railhead damage.

In Simpack, two approaches are available to calculate the normal wheel–rail contact tractions. The first is an equivalent elastic contact model based on Hertzian contact theory [48]. The second is the discrete elastic contact method based on the semi-Hertzian

STRIPES approach [49, 50], which can also account for material plasticity. The tangential contact problem is solved using the FASTSIM algorithm [51], which is modified when it is combined with the discrete elastic contact method. The different contact methods are described in Section 3.3. Up to five contact patches can be active simultaneously in the simulation.

3.3 Wheel–rail contact modeling

The wheel–rail contact generates a complex stress field that comprises both a normal component, mainly resulting from the vertical wheel load, and tangential components, which result from creepage. In numerical modeling, accurately capturing the shape, magnitude, and distribution of these contact stresses is crucial to evaluating the railhead degradation.

In detailed contact analyses, such as those using FE models or Kalker's CONTACT program [52, 53], normal and tangential contacts are typically solved in combination. However, for elastic contact problems, tangential tractions have a minor effect on the normal pressure distribution and contact area [54]. Therefore, a common approach is to solve the contact problem sequentially. First, the normal contact problem is addressed to determine the contact area and pressure distribution. Then, the tangential problem is solved to compute the tangential tractions and slip distribution within the contact patch. The total contact stresses are obtained by superimposing the tangential tractions onto the normal pressure field.

The normal contact problem can be solved with a wide range of models as has been proposed in the literature, see e.g. [53–55], each offering different levels of complexity and accuracy. In this thesis, the scope is restricted to contact models that are either available within the MBD software Simpack or the Hertzian-inspired metamodel developed by Skrypnyk et al. [24].

Hertz contact theory [48] is an analytical solution that is widely used due to its simplicity and computational efficiency. The theory considers an elliptical contact patch with semi-axes a and b and a semi-elliptical normal contact traction distribution t_n that reaches its maximum p_n at the contact patch center, as illustrated in Figure 3.2a. The distribution is defined as

$$t_\mathrm{n}(x,y) = p_\mathrm{n}\sqrt{1-\left(\frac{x}{a}\right)^2-\left(\frac{y}{b}\right)^2}, \quad |x|<a, \quad |y|<b, \tag{3.1}$$

where x and y are local coordinates within the elliptical contact patch.
For the Hertzian contact to be valid, the following assumptions must be true:

- *Homogeneous, isotropic and linear elastic materials:* This implies small strains.
- *Half-space assumption:* The contact dimensions (a and b) are much smaller than the contacting bodies' dimensions and radii of curvature.
- *Non-conformal contact:* The contacting surfaces have different curvatures, resulting in a small contact area relative to body dimensions.

- *Constant curvature:* The contacting surfaces have constant curvatures, producing an elliptical contact patch.
- *Smooth surfaces.*
- *Quasi-identity or frictionless surfaces*: no shear stresses are generated.

These assumptions are often violated in wheel–rail contact. For high axle loads or during braking or slipping, plastic deformation can occur. For worn profiles, tight curves, or flange contact situations, the surfaces can become conformal with non-elliptical contact areas. Additionally, real wheel and rail surfaces are rarely perfectly smooth or frictionless, which affects creep forces and tangential contact behavior. These violations motivate the use of more advanced contact models.

The semi-Hertzian contact model STRIPES, developed by Ayasse et al. [49] and Quost et al. [50], addresses some of these issues. It retains computational efficiency while improving accuracy for cases where the conformity or constant curvature assumptions of Hertz theory are not valid. The method accounts for variations in the lateral curvature by dividing the contact area into longitudinal strips, as illustrated in Figure 3.2b. In each strip, the normal stress distribution is calculated using a Hertzian-based formula along the rolling (longitudinal) direction. STRIPES have also been extended by Sebès et al. [56] and Chevalier et al. [57] to work for high-load cases where stresses exceed the elastic limit by incorporating perfect material plasticity. In this extension, a simplified von Mises yield criterion is applied at the center of each strip m to ensure that the local contact pressure p_{n}^{m} does not exceed the yield threshold detailed in [56]. As a result, the predicted contact area increases and the peak pressures are reduced compared to a purely elastic calculation. Nevertheless, the perfect-plastic assumption neglects material hardening and can therefore underestimate contact stresses.

The Hertzian-inspired metamodel by Skrypnyk et al. [24] addresses this limitation by incorporating elasto-plastic material behavior with hardening in the rail, while modeling the wheel as linearly elastic. Compared to STRIPES, this leads to more realistic predictions under high-load conditions. The model is calibrated based on 3D FE simulations of the normal contact problem with elasto-plastic rail behavior. However, it relies on the Hertzian assumption of *constant curvature* radii near the contact point, which limits its applicability to elliptical contacts. On the other hand, this symmetry allows the FE analyses to be performed on only a quarter of the domain, see Figure 3.2c. Computational efficiency is achieved by calibrating a few model coefficients against these FE simulations for a representative range of contact scenarios. However, this also makes the model's accuracy dependent on the quality of the calibration data. Once calibrated, the metamodel uses the local contact radii and applied normal contact force from the MBD simulations as inputs to predict the contact patch dimensions, maximum contact pressure, and maximum von Mises stress.

Tangential contact models describe how wheel–rail forces arise from creepage. Carter [27] and Fromm [28] established how tangential tractions vary within the contact patch and introduced the concept of stick and slip regions (see Section 2.1). In the slip region, the tangential $t_{\mathrm{t}}(x, y)$ and longitudinal $t_{\mathrm{x}}(x, y)$ traction is bounded by Coulomb's friction

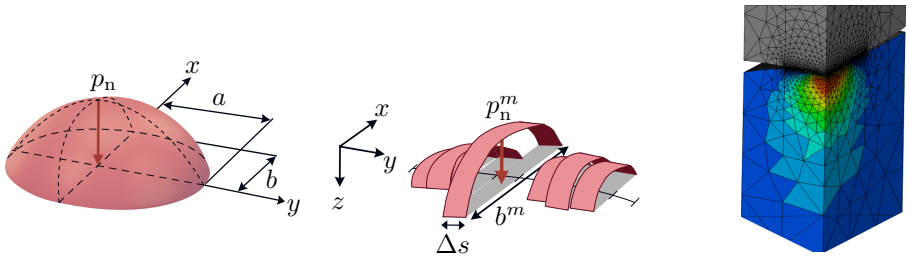

(a) Hertz *(b) STRIPES* *(c) Metamodel*

Figure 3.2: *Normal contact models used in this thesis. (a) Hertzian solution assuming an elliptical contact patch, (b) the semi-Hertzian approach STRIPES, which divides the contact into longitudinal strips to account for curvature variations, and (c) a representative 3D elasto-plastic FE analysis used in the calibration of the Metamodel.*

limit as

$$\sqrt{t_{\mathrm{t}}^2(x,y) + t_{\mathrm{x}}^2(x,y)} < \mu t_{\mathrm{n}}(x,y), \tag{3.2}$$

where t_n is the normal surface contact traction distribution and μ is the friction coefficient. In the stick region, the traction is reduced by a counteracting smaller elliptic traction bound. However, Carter and Fromm's theories were formulated as 2D line-contact problems assuming pure longitudinal creepage and plane strain. These simplifications neglect lateral and spin creepages that also occur in realistic rolling conditions.

To address these limitations, more general 3D rolling-contact models have been developed, such as Kalker's theories [51, 52, 58]. His formulations extend Carter and Fromm's concepts and range from simplified models to more exact ones, and are reviewed in [59]. His complete theory, implemented in the program CONTACT [58], provides highly accurate predictions for all combinations of creepage and spin between two elastic bodies, but is computationally demanding.

To improve computational efficiency, Kalker developed the simplified rolling-contact algorithm FASTSIM [51]. The model assumes that local surface displacements are proportional to the tangential tractions, which are saturated by Coulomb's limit. Within this contact theory, the contact patch is divided into rectangular elements. Although originally derived for elliptical contact areas using elastic parameters derived from Kalker's Linear Theory [60], FASTSIM has since been extended to handle non-elliptical contact shapes. In the STRIPES method, for instance, the contact area is divided into longitudinal strips (see Figure 3.2b), and virtual local ellipses are assigned to each strip. These virtual ellipses provide the input needed to evaluate the elastic parameters [61], which are then applied to compute the tangential tractions strip by strip.

3.4 Elasto-plastic FE modeling

When studying the long-term mechanical response of rails under repeated wheel passages, FE modeling with cyclic plasticity for material behavior provides a way to capture the

accumulation of plasticity in the railhead. A cyclic plasticity model can predict phenomena such as the Bauchinger effect, ratcheting, plastic shakedown, and cyclic hardening or softening.

Full 3D models are the most accurate way to model evolving plasticity, see e.g., [62–67], since they resolve the complete stress-strain history within the rail, but are computationally demanding, which makes them impractical for many wheel overrollings. Simplified 2D FE analyses, such as the plane-strain one used in [13, 44, 45] and **Paper A**, or the 2D generalized plane strain model in [68, 69], are far more efficient but can only approximate the contact stress distribution and miss important 3D effects, such as Poisson's effects in the rail, and longitudinal stress propagation, which is needed to accurately predict mechanisms such as crack initiation planes. Therefore, a ROM framework was developed in **Paper D** and **Paper E**, which is described in Chapter 4. The framework retains the accuracy of 3D analyses while drastically reducing computational cost.

Thus, this thesis uses both the ROM framework in **Paper D** and **Paper E** and simplified 2D analyses in **Paper A** to model evolving plasticity. The simplified 2D model consists of a 2D nonlinear FE model assuming plane strain to investigate plastic strain accumulation. To compensate for the lack of a full 3D contact description, the applied maximum normal force per unit length was adjusted for each loading case such that the maximum von Mises stress in the 2D model matches the one predicted by the Hertzian-inspired metamodel (see Section 3.3). Tangential traction is incorporated by assuming full slip, and the resulting plastic strains are computed in the 2D cross-section. To make the simulations computationally feasible for many load cycles, the nonlinear FE analysis, including plasticity evolution, is extrapolated using the procedure of [70].

When modeling long-term damage, it is crucial to use a constitutive model that can capture the cyclic behavior of the material and predict its mechanical response under repeated loading. The response can be modeled using a variety of cyclic plasticity models, as discussed in the literature [71, 72]. The models differ in their choice of kinematic and isotropic hardening laws and whether they include additional effects. Kinematic hardening translates the yield surface to capture phenomena such as ratcheting and the Bauschinger effect, while isotropic hardening expands or contracts the yield surface to represent cyclic hardening or softening.

In this thesis, the Ohno-Wang [73] nonlinear kinematic hardening model is adopted, assuming small strains, a von Mises yield criterion, and linear isotropic elasticity. Isotropic hardening is neglected since kinematic hardening is often dominating for pearlitic rail materials (see e.g., [44, 70]). The evolution of each backstress $\dot{\boldsymbol{\alpha}}_i$ is given by

$$\dot{\boldsymbol{\alpha}}_i = \frac{2}{3}\, C_i\, \dot{\boldsymbol{\epsilon}}^{\mathrm{p}} - \frac{\gamma_i^{m_i+1}}{C_i^{m_i}} \left(\sqrt{\frac{3}{2}} |\boldsymbol{\alpha}_i| \right)^{m_i} < \dot{\boldsymbol{\epsilon}}_{\mathrm{p}} : \boldsymbol{\alpha}_i > \sqrt{\frac{2}{3}} \frac{\boldsymbol{\alpha}_i}{|\boldsymbol{\alpha}_i|}, \tag{3.3}$$

where $\dot{\boldsymbol{\epsilon}}^{\mathrm{p}}$ is the plastic strain rate, C_i, γ_i, and m_i are material parameters for each backstress i, and the Macaulay bracket $< \bullet >$ is defined as $< \bullet >= 0.5\ (\bullet + | \bullet |)$. The constitutive relations are presented in more detail in **Paper D** and [74].

The material parameters listed in **Paper A** and **Paper D** were calibrated against two uniaxial stress-controlled cyclic loading tests on rail grade R260 from Ahlström et al. [75]. In the experiments, almost no isotropic hardening was observed, which again motivates why it was neglected in the material modeling. Three backstresses were sufficient to

reproduce the experimentally observed ratcheting behavior. In this thesis, the material model is applied both in the Hertzian-inspired metamodel and for evaluating railhead damage in terms of accumulated plastic deformation.

3.5 Wear modeling

Wear constitutes one of the primary degradation mechanisms in the wheel–rail system, particularly in curves. This can result in significant material removal over time, thus changing the rail profile substantially. Therefore, accurate wear modeling is important to predict the evolution of the rail profile.

Two main approaches are commonly used to model wear. The first type of model is based on energy dissipation and relates wear to the frictional energy lost in the contact patch. The second type of model is based on sliding distance according to Archard [76] and is proportional to the product of normal load and sliding distance. A review of these models can be found in [77].

In energy dissipation-based models, wear is assumed to be proportional to mechanical energy lost as heat due to factors such as friction. At the global level, the rate of energy dissipation $\bar{E}$ in the contact can be estimated as

$$\bar{E} = F_{\mathrm{x}}\nu_{\mathrm{x}} + F_{\mathrm{t}}\nu_{\mathrm{t}} + M\phi, \tag{3.4}$$

where F_{x} and F_{t} are the longitudinal and lateral creep forces, M is the spin moment, and ν_{x}, ν_{t}, and ϕ are the corresponding creepages and spin. Several wear models are based on this concept, often incorporating empirical fits between $\bar{E}$ and observed wear rates [78–80]. Although energy dissipation concepts are simple and can be refined, many different combinations of creep forces and creepages can result in the same value of $\bar{E}$. Thus, it is not always clear that material removal correlates uniquely with this single quantity.

Instead, Archard's wear model [76] relates the wear volume V to the normal contact force F_{N} and sliding distance d as

$$V = k\frac{F_{\mathrm{N}}\, d}{H}, \tag{3.5}$$

where k is the wear coefficient, and H is the hardness of the softer of the two materials in contact. Jendel [81] extended this formulation to incorporate local contact conditions within the patch. The area is discretized using the FASTSIM algorithm [51], which provides local distributions of contact pressure and relative sliding distance, from which the wear depth distribution can be obtained. However, Archard's model does not explicitly capture the influence of frictional energy dissipation, temperature effects, or strain-hardened materials [82]. Nevertheless, Archard-based approaches are well established in railway applications, see e.g., [81, 83–85], and this model has been used in **Paper A**-**Paper C**. Further details of the implementation are given in **Paper C** and in [86].

Both the energy dissipation and Archard formulations require a wear coefficient. The value of this coefficient is difficult to determine because it depends on the material pair, loading conditions, temperature, lubrication, and contamination in the contact. The

simplest approach is to assign a constant (global) coefficient, as was done in **Paper A** and **Paper B**. While this approach is straightforward, it may not yield sufficiently accurate results. One refinement is to allow the coefficient to vary linearly with sliding velocity, as proposed in Brouzoulis et al. [84], thereby capturing some of the observed dependence on loading conditions. Another alternative is the wear map introduced by Jendel [81] for use with Archard's law. This map defines different wear regimes (and thus different coefficients) as a function of contact pressure and sliding distance (see Figure 3.3). Such maps can more accurately represent transitions between mild, severe, and catastrophic wear, but they are material-specific and can only be determined in principle under idealized laboratory conditions (e.g., dry pin-on-disc or disc-on-disc experiments). Therefore, their applicability to real railway environments, where weather, lubrication, and contamination can strongly influence wear, is limited. For this reason, calibration against field measurements is often required, as discussed in Section 3.7.

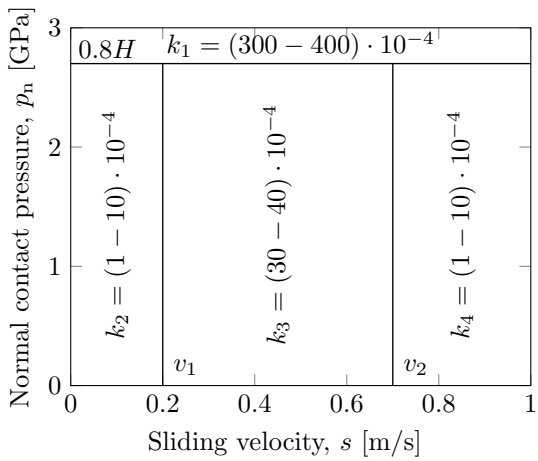

Figure 3.3: *Wear map for dry conditions with different wear regimes as a function of contact pressure and sliding velocity, based on [81].*

3.6 Surface rolling contact fatigue prediction

Rail surface damage caused by RCF typically initiates at the gauge corner and is a major problem since it is driving a lot of track maintenance [87]. A wide range of models have been proposed to predict the initiation of surface cracks in rails. See, for example, [31, 88, 89] for reviews. Models based on the ratcheting failure mechanism describe how repeated loading leads to a gradual accumulation of plastic strain and, ultimately, to the initiation of RCF cracks [5, 90]. Energy-based models, on the other hand, relate fatigue damage to the dissipated energy (see Section 3.5) in the contact [91, 92], while microstructure-based models incorporate material microstructure into the fatigue damage predictions [16, 93, 94]. Shakedown-based methods identify operating conditions where

surface plasticity or ratcheting is expected, thereby linking contact loads to crack initiation risk [95–97]. Finally, multiaxial fatigue criteria such as the Dang Van formulation [98] or the Jiang-Sehitoglu formulation [99] are often used to identify critical crack planes from local stress-strain histories. These models are typically combined with MBD simulations to provide realistic contact conditions or with elasto-plastic FE analyses (see Sections 3.4 and 4) to improve the accuracy of local stress-strain predictions [69, 100].

In **Paper A**, a simplified method is used that circumvents the need for revolved local stress and strains within the rail. The method combines the shakedown theory [95] and the energy dissipation model [91] through a distributed RCF index proposed by Nielsen et al. [86]. In accordance with the framework, the surface index FI_{surf} sets out from the shakedown map and was in [97] formulated as

$$FI_{\text{surf}} = \frac{\sqrt{F_{\text{x}}^2 + F_{\text{t}}^2}}{F_{\text{N}}} - \frac{2\pi ab\tau}{3F_{\text{N}}} \tag{3.6}$$

where F_{x}, F_{t} and F_{N} are the contact forces (see Figure 2.2), a and b are the semi-axes of the Hertzian contact patch (see Figure 3.2a), and τ denotes the shear yield stress. Surface fatigue is predicted when $FI_{\text{surf}} > 0$. A penalty function $f_{\text{p}}(\bar{E})$ is applied to reduce FI_{surf} at large values of dissipated energy $\bar{E}$ (neglecting spin), since high energy dissipation also leads to wear, which tends to remove cracks from the surface [91]. The turning points of this function are determined by the contact area and the material properties of the rail grade. Partial slip is incorporated by computing local damage in each element of the discretized contact patch using FASTSIM [51]. The distributed index is then accumulated over load cycles according to the Palmgren-Miner rule, with crack initiation assumed once the value reaches one. Thus, this criterion provides an estimation of the risk of crack initiation while capturing the influence of partial slip and the interaction with wear through energy dissipation.

3.7 Model Calibration

Within a digital twin framework, model calibration is essential to ensure the consistency between numerical predictions and field observations. Calibration involves adjusting model parameters, e.g., wear coefficients and yield limits, so that the simulated response accurately replicates the observed field behavior, such as railhead material degradation. This process improves the reliability of predictions of future events.

Calibration is often formulated as an optimization problem, wherein a set of model parameters $\boldsymbol{\alpha}$ are tuned to minimize the discrepancy between simulated $f(\boldsymbol{\alpha})$ and measured f^{meas} response through a loss function $\mathcal{L}$ (e.g., normalized squared error). The optimal parameter set $\boldsymbol{\alpha}^{\text{opt}}$ is then obtained as

$$\boldsymbol{\alpha}^{\text{opt}} = \arg\min_{\boldsymbol{\alpha}} \mathcal{L}\big(f(\boldsymbol{\alpha}), f^{\text{meas}}\big), \tag{3.7}$$

In this thesis, the calibration targets f include the material degradation indicators discussed in Section 2.4 as well as in **Paper A** and **Paper C**.

Different optimization strategies can be used, depending on the complexity of the problem and available computational resources. The simplest approach relies on manual

tuning, where parameters are varied one at a time, and the resulting model response is compared with field data. This method was used in **Paper A**, where global wear coefficients and yield limits were tuned against area-based measures to better capture the accumulated wear and plastic deformation observed in the field. In **Paper B**, the same calibrated wear coefficient was used, while model parameters related to track and vehicle setup, as well as the contact formulation in the MBD simulations, were adjusted. This was done to improve the agreement between simulated and measured rail profile change distributions. Although this calibration approach used in **Paper A** and **Paper B** improved the model accuracy, it is computationally costly for tuning multiple parameters, and it does not guarantee optimal results.

To address these limitations, **Paper C** adopts a more systematic calibration procedure focusing on the wear coefficients within the wear map [81] described in Section 3.5. Previous studies have used various strategies for calibration of this map, including adjusting scaling factors and regime boundaries [83], introducing linear variations of the wear coefficient with the sliding velocity [84], or performing extensive simulations followed by parameter fitting [14, 101]. Other authors, such as Ye et al. [102] and Wen et al. [103], reduced computational cost by introducing surrogate models for the calibration problem.

Paper C also uses surrogate models for calibrating the wear map, but in this case for a STRIPES contact formulation [49, 50] rather than the classical Hertzian contact [48]. Although the STRIPES approach has been reported to influence wear modeling significantly [104, 105], it has not previously been investigated in the context of calibration of the wear map. Surrogate models are particularly useful when the evaluation of $f(\boldsymbol{\alpha})$ is computationally expensive, as they eliminate the need for repeated full simulations during the optimization loop. To construct the surrogates, full wear simulations are performed on parameter sets sampled using Latin Hypercube Sampling (LHS) [106]. The accuracy of the surrogate models depends on how representative the training data is, making it crucial to cover the relevant parameter ranges of the wear coefficients and include enough samples.

The choice of the surrogate model is also important. Polynomial regression is simple but limited for nonlinear problems. Radial Basis Functions [107] are more flexible but sensitive to kernel choice and scaling, while Neural Networks, as used in [102, 103], can model highly nonlinear relationships at a large scale but require extensive data and careful tuning. In this thesis, Gaussian Process Regression (GPR) [108] is used with an exponential squared kernel of Automatic Relevance Determination (ARD). GPR is a robust technique that can model nonlinear and noisy responses, provide smooth approximations even with relatively small training sets, and deliver predictive uncertainty. The ARD kernel also quantifies the relative importance of each input parameter by assigning individual length scales in the covariance function.

Once validated, the surrogate models can be efficiently optimized according to (3.7). As with surrogate choice, many optimization methods are available, and the best option depends on the characteristics of $f(\boldsymbol{\alpha})$. In this work, where the evaluation of the surrogate is inexpensive, the global optimization algorithm Particle Swarm Optimization (PSO) is first used to explore the parameter space and avoid getting stuck in a local minimum. The best solution from PSO is then passed as an initial guess to a local gradient-based method, an interior-point algorithm, to refine the result.

4. Numerical model reduction for evolving rail plasticity

This chapter introduces a Reduced Order Modeling (ROM) framework for efficient prediction of 3D evolving railhead plasticity under moving contact loads. The approach combines a steady-state formulation, an iterative scheme to handle the coupling between solving plastic strains and displacements, and the Proper Generalized Decomposition (PGD) method to efficently compute the displacement field.

4.1 Overview of the reduced-order modeling framework

Accurately predicting railhead damage from repeated wheel passages requires determining the 3D stress–strain history within the rail. However, full 3D FE analyses, such as those in [62–67], are computationally expensive. Simplified 2D models, as used in [44, 68, 69], are more efficient but miss key 3D effects that influence crack initiation and growth, such as Poisson's effects in the railhead, and longitudinal traction. To combine the accuracy of 3D modeling with the efficiency of 2D approaches, a ROM framework was introduced in **Paper D** and **Paper E**.

The ROM framework reproduces the fidelity of a full 3D description while substantially reducing the computational cost compared to conventional 3D FE analyses. The framework, illustrated in Figure 4.1, incorporates the elasto-plastic behavior of the railhead through three main components.

1. A *steady-state assumption* is introduced for the moving contact loads by adopting a convective coordinate system that follows the contact along the railhead. This transforms the moving contact problem into a stationary formulation, where the material history is tracked along streamlines in the spatial mesh. This way, only one load increment is needed, and the plastic strain computations can be carried out in parallel at each integration point of the railhead cross-section, significantly improving efficiency.
2. An *iterative (decoupled) scheme* is applied to manage the coupling between the displacement and plastic strain fields.
3. The *PGD method* is used, which enables a domain decomposition of the 3D mesh and a parametrization of the contact load to provide a more efficient solution of the displacement field.

Once convergence is reached, the process is repeated for subsequent overrollings. The detail of each part is presented in the following sections.

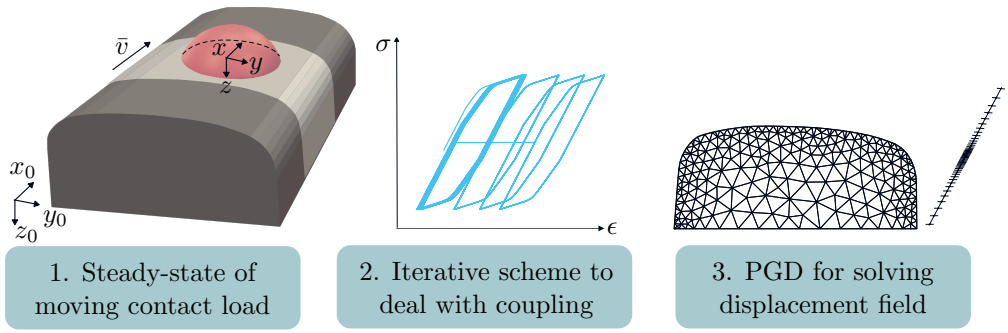

Figure 4.1: *Schematic of ROM framework for evolving railhead plasticity. The framework consists of three main parts.*

4.2 Steady-state formulation for moving contact loads

In analyses of moving contact problems, conventional 3D FE simulations are often carried out in a Lagrangian frame (see, e.g., [64–67, 109]). This formulation uses a fixed spatial coordinate system $\boldsymbol{x}_0 = (x_0, y_0, z_0)$, as illustrated in Figure 4.2a. In this system, the material points and their paths are tracked directly, as the computational mesh moves with the material. The advantage of the Lagrangian description is its ability to directly represent material deformation and evolving boundaries. However, this approach has limitations when applied to moving contact loads. The load must be advanced step by step across the mesh, requiring a large number of increments. Moreover, accurately capturing the stresses and strains of nonlinear materials requires both long domains and a refined mesh near the contact surface. This refined mesh cannot be restricted to a small region; rather, it must extend over a large portion of the domain. Therefore, the computational cost increases substantially, which makes Lagrangian simulations cumbersome when many overrollings are considered.

In contrast, an Eulerian frame uses a fixed spatial grid and monitors how material flows through stationary points. While effective for many fluid dynamics applications, the approach is less suitable for problems with moving boundaries, such as fluid–structure interaction or rolling contact problems.

To combine the advantages of Lagrangian and Eulerian descriptions, the Arbitrary Lagrangian–Eulerian (ALE) formulation was introduced by Donea et al. [110] and Hughes et al. [111] for fluid–structure interaction problems. In an ALE framework, the mesh can move with the material (as in the Lagrangian description), remain fixed in space (as in the Eulerian description), or move in an arbitrary manner independent of the material [112]. This flexibility makes it particularly advantageous for rolling contact problems, as it enables the mesh to track the moving load and accommodate material flow.

The use of ALE for rolling contact problems has been explored extensively in the literature. Nackenhorst [113] first applied the ALE method to steady-state 3D rolling

elastic contact with large deformations, modeling tire–pavement interaction where the tire is deformable and the pavement is assumed rigid. He later provided the theoretical foundation for ALE formulations for more general rolling elastic contact in [114]. Damme et al. [115] extended the framework to rail–wheel contact, accounting for deformations in both bodies.

Subsequent studies introduced nonlinear material behavior in rolling contact analyses. Chang et al. [85] simulated wheel–rail rolling contact using a nonlinear material model. Wollny et al. [116, 117] analyzed inelastic tire–pavement interaction. More recently, Anantheswar et al. [118, 119] included transient effects from tire loads such as acceleration, braking, and variations in load amplitude. However, when nonlinear material behavior is included as in these studies, additional complications arise. Because state variables are not tied to fixed integration points, they must be mapped between the initial (Lagrangian) configuration and the current (deformed) configuration in a convective manner. This remapping increases computational cost, complicates the update of material tangents, and may introduce numerical instabilities due to the convective term.

In this thesis, we adopt a simpler alternative to the ALE approach presented in **Paper E**. A convective coordinate system $\boldsymbol{x} = (x, y, z)$ is introduced that translates with the moving contact load along the rolling direction in the *undeformed* configuration, as illustrated in Figure 4.2b. We note that this simplification renders the material time derivatives explicit in the prescribed convection. Another effect is that the convected domain, illustrated in Figure 4.2b, deforms with the solution even at in- and outflow boundaries. By formulating the problem in this moving frame and assuming a steady-state response, the load becomes stationary, reducing the solution to a single increment. The computational domain can thus be restricted to a compact region surrounding the contact patch, which reduces the cost further. This approach has been successfully applied to inelastic deformation in pavements by Shen and Kirkner [120], in rails by Dang Van et al. [121–123], and to transient elastic wheel–rail contact by Draganis et al. [124].

In the convective frame, the stationary rolling response becomes time-independent and is instead expressed as a spatial variation along streamlines of the FE mesh. Thus, the material history is traced along the prescribed convected velocity along streamlines of the FE mesh. At each integration point, the state variables are updated by reading the history of the preceding point along the streamline, as done in previous steady-state formulations [117, 121–123, 125]. Figure 4.2b illustrates this concept: material flows into the domain at the right (inflow) boundary, moves through the mesh in the opposite direction to the moving load, and leaves the domain at the left (outflow) boundary. Thereby, the plastic strain field $\boldsymbol{\epsilon}^{\mathrm{p}}$ can be obtained as

$$\boldsymbol{\epsilon}^{\mathrm{p}}(x, y, z) = f[\boldsymbol{u}(x, y, z), \boldsymbol{\epsilon}^{\mathrm{p}}_{\mathrm{in}}(y, z)], \tag{4.1}$$

where $\boldsymbol{u}$ is the displacement field and $\boldsymbol{\epsilon}^{\mathrm{p}}_{\mathrm{in}}$ is the prescribed plastic strain at the inflow boundary. For brevity, the representation in (4.1) omits additional internal variables that are included in the full formulation presented in **Paper E**. Because each streamline in the cross-section can be solved independently, the formulation allows for efficient parallel computation.

Turning to the balance of momentum, the analysis is restricted to a quasi-static response. Furthermore, small deformations are assumed, and the material is modeled as linear

elastic–plastic, based on the additive decomposition of the elastic and plastic strains. The weak form for the displacement field can then be expressed as

$$a(\boldsymbol{u}, \delta\boldsymbol{u}) - b(\boldsymbol{\epsilon}^{\mathrm{p}}, \delta\boldsymbol{u}) = l(\boldsymbol{q}; \delta\boldsymbol{u}) \quad \forall \delta\boldsymbol{u} \in \mathbb{U}, \tag{4.2}$$

where $\delta\boldsymbol{u}$ a test function in the admissible space $\mathbb{U}$ and $\boldsymbol{q}$ is a prescribed load scenario. A detailed description of the governing equations is provided in **Paper E**.

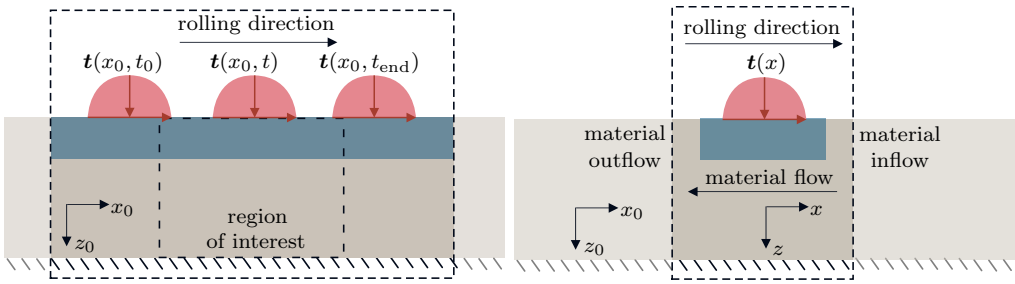

(a) *Lagrangian frame* ***(b)*** *Convective coordinate system frame*

Figure 4.2: *Illustration of moving surface traction* $\boldsymbol{t}$ *in (a) the Lagrangian frame* $\boldsymbol{x}_0 = (x_0, y_0, z_0)$*, requiring a long domain and multiple increments* t*, and (b) the convective frame* $\boldsymbol{x} = (x, y, z)$*, where the load is stationary and material flows into the domain at the right boundary and exits at the left. The blue area denotes the refined mesh region.*

4.3 Iterative solution of coupled displacement and plastic strain fields

It is apparent that the single overrolling problem in (4.1) and (4.2) is coupled. The displacement field governs the evolution of plastic strains, while the accumulated plastic strains contribute to the overall deformation. Although this coupling can be resolved monolithically, the present work adopts an iterative (decoupled) solution strategy to reduce both implementation complexity and computational cost.

Several iterative techniques can be used for such problems, including Newton, Newton–Raphson, and fixed-point methods. Each approach involves trade-offs between convergence rate, robustness, and computational expense. Newton-type methods exhibit rapid (quadratic) convergence when the initial guess lies sufficiently close to the true solution. However, they require gradient evaluations and tangent stiffness updates, which increase computational cost, and they may fail if the initial estimate is poor [126]. Fixed-point iterations, on the other hand, typically have a slower convergence rate (linear) but avoid the computation of the Jacobian. For the studied problem, an evaluation of the full Jacobian would increase the complexity of (4.1), making fixed-point iterations an attractive alternative.

To further reduce the computational complexity, the linearity of (4.2) allows an additive decomposition of the displacement field. Specifically, the total displacement $\boldsymbol{u}$ can be

expressed as the sum of an elastic contribution $\boldsymbol{u}^{\mathrm{e}}[\boldsymbol{q}]$, driven by the applied load $\boldsymbol{q}$, and a plastic contribution $\boldsymbol{u}^{\mathrm{p}}[\boldsymbol{\epsilon}^{\mathrm{p}}]$, induced by the plastic strain field $\boldsymbol{\epsilon}^{\mathrm{p}}$

$$\boldsymbol{u} = \boldsymbol{u}^{\mathrm{e}}[\boldsymbol{q}] + \boldsymbol{u}^{\mathrm{p}}[\boldsymbol{\epsilon}^{\mathrm{p}}]. \tag{4.3}$$

Substituting this decomposition into (4.2) yields two uncoupled linear subproblems

$$a(\boldsymbol{u}^{\mathrm{e}}, \delta\boldsymbol{u}) = l(\boldsymbol{q}; \delta\boldsymbol{u}) \quad \forall \delta\boldsymbol{u} \in \mathbb{U}, \tag{4.4a}$$
$$a(\boldsymbol{u}^{\mathrm{p}}, \delta\boldsymbol{u}) = b(\boldsymbol{\epsilon}^{\mathrm{p}}, \delta\boldsymbol{u}) \quad \forall \delta\boldsymbol{u} \in \mathbb{U}. \tag{4.4b}$$

This decomposition effectively decouples the elastic and plastic contributions, allowing each contribution to be solved independently[1]. An important advantage of the adopted formulation is that it avoids the complex remapping of state variables typically required in ALE formulations, since the convective term in (4.1) is independent of $\boldsymbol{u}$.

For this formulation, a fixed-point iterative scheme is utilized, where the plastic strain and displacement fields are updated in an alternating manner until convergence is achieved. At each iteration, the plastic strain field in (4.1) is first updated based on the state variables at the inflow boundary, together with a known displacement field in the entire domain. The corresponding permanent displacement contribution $\boldsymbol{u}^{\mathrm{p}}$ is then computed from (4.4b) based on the updated plastic strains. This procedure is repeated until the prescribed convergence criterion is achieved.

The elastic displacement $\boldsymbol{u}^{\mathrm{e}}$ obtained from (4.4a), which depends solely on the applied load and the linear elastic material response, can be precomputed for each loading scenario. Thus, only (4.1) and (4.4b) need to be performed iteratively, which substantially reduces the computational cost. Each displacement contribution can be obtained either from a full 3D FE solution or, to further reduce the computational cost, from a ROM using the PGD method, as described in the next section.

4.4 Proper Generalized Decomposition for displacement field computation

ROMs are used to reduce the computational complexity of high-dimensional, multiphysics, or parametric problems. By constructing low-dimensional approximations of full-order models, projection-based ROMs enable efficient computations while retaining sufficient accuracy. This approach preserves the physical fidelity of the original equations while significantly lowering computational cost. ROMs are particularly useful in applications requiring repeated evaluations, such as parametric analyses, optimization, or real-time simulations.

A wide range of model-reduction techniques has been proposed in the literature. Among them are the *a posteriori* approaches such as Proper Orthogonal Decomposition (POD) [20, 127, 128], Principal Component Analysis (PCA) [21, 129], and Singular Value Decomposition (SVD) [130, 131]. These techniques rely on a set of precomputed full-order

[1]The plastic contribution $\boldsymbol{u}^{\mathrm{p}}[\boldsymbol{\epsilon}^{\mathrm{p}}]$ represents the solution to (4.4b), and not a potential for the plastic strain, i.e., $\boldsymbol{\epsilon}^{\mathrm{p}} \neq \boldsymbol{\epsilon}[\boldsymbol{u}^{\mathrm{p}}]$ □.

solutions, or *snapshots*, obtained for different parameter values [23]. In POD, these snapshots are used to construct an orthonormal reduced basis that captures the main features of the full problem. The approximation of a field variable u then reads

$$u(\boldsymbol{x}, \eta) \approx \sum_{i=1}^{N_\mathrm{R}} \varphi_i(\boldsymbol{x}) \xi_i(\eta), \tag{4.5}$$

where $\varphi_i(\boldsymbol{x})$ are the (modal) basis functions of $\boldsymbol{x}$, $\xi_i(\eta)$ are the associated modal coefficients that depend on the parameters η. The number of retained modes N_R is much smaller than the number of degrees of freedom of the full problem N_full, i.e., $N_\mathrm{R} \ll N_\mathrm{full}$. For new parameter values η, the coefficients $\xi_i(\eta)$ can be computed (in an online phase) through projection or interpolation onto the reduced basis.

While these *a posteriori* methods offer compact and efficient representations of the data, their dependence on precomputed snapshots can make them impractical for problems with large parameter spaces or when the full solution cannot be generated in advance. The generation of a sufficiently rich snapshot set becomes computationally expensive, e.g., when the underlying problem involves many parameters.

To overcome these limitations, the PGD method [22, 132, 133] adopts an *a priori* strategy. Unlike POD, which builds a reduced basis from precomputed full-order solutions, PGD constructs the reduced representation directly during the solution process [22]. This eliminates the need for any preexisting snapshots, and PGD can also accommodate additional coordinates, such as material or load parameters, by incorporating these parameters as extra dimensions of the problem [23]. PGD has therefore been successfully applied to a broad range of high-dimensional [132–135] and parametric problems [23, 136–140]. For high-dimensional problems, PGD mitigates the curse of dimensionality by ensuring the solution complexity scales linearly with the dimension of the subproblems [135]. Ammar et al. [132] demonstrated this capability for steady-state fluid flows and later extended the formulation to transient effects [133]. The accuracy of PGD solutions was further analyzed in [134], while Chinesta et al. [135] reviewed its advances in multidimensional modeling. For parametric analyses, PGD allows a single offline solution to represent the entire parameter space by incorporating parameters as additional coordinates. This makes it possible to evaluate the model for arbitrary parameter values without recomputation. Reported applications include the treatment of material parameters as in [136–139], or boundary conditions considered in [22, 140].

The central idea of PGD is to approximate the solution as a finite sum of *separable* functions, where each function depends on a subset of coordinates or parameters x^k (e.g., spatial coordinates, time, or load parameters). Exploiting this separability, a generic field $u(x^1, \ldots, x^K)$ expressed in K-dimensional input can be represented as

$$u(x^1, \ldots, x^K) \approx \sum_{n=1}^{N} \prod_{m=1}^{K} X_n^k(x^k), \tag{4.6}$$

where X_n^k are the unknown separated (modal) functions that define the nth mode. The approximation is enriched incrementally by adding one separable mode at a time until convergence is achieved or the prescribed number of modes N is reached.

A common feature of many ROM techniques is the *offline-online* strategy, which separates the computationally intensive tasks from those that can be performed efficiently. In POD, the offline phase involves solving the full-order problem for several parameter sets, collecting snapshots, and forming a reduced basis via orthogonal decomposition. PGD follows a similar structure, but the offline phase instead involves computing all separable modes across the entire parameter domain, as in (4.6). Once obtained, these modes enable rapid online evaluation of particular solutions for any combination of parameters. This separation is highly advantageous when the dimensionality of the parameter space is high but limited. However, in contrast to POD, PGD can also be used directly in the online stage, providing approximate solutions without the need for an offline database or prior data collection.

In **Paper D** and **Paper E**, PGD was applied to efficiently approximate the displacement field described in (4.3) and (4.4) by using a domain decomposition and a parametrization of the distributed surface load. Following the domain decomposition approach proposed in Bognet et al. [141, 142] and Giner et al. [138], the railhead is represented by a 2D in-plane cross-section $\boldsymbol{y} = (y, z)$ and a one-dimensional out-of-plane discretization x, treated as parameters in the separated representation. This decomposition is illustrated in the second step of Figure 4.1. Thus, the displacement field $\boldsymbol{u}(\boldsymbol{y}, x)$ is expressed as

$$\boldsymbol{u}(\boldsymbol{y}, x) \approx \sum_{n=1}^{N} \boldsymbol{Y}_n(\boldsymbol{y})\, X_n(x), \tag{4.7}$$

where $\boldsymbol{Y}_n$ are 3D vector field defined on a 2D domain and X_n are scalar functions on a 1D domain. Since the computational effort is dominated by solving the functions for $\boldsymbol{Y}_n$, the effective cost is comparable to that of a 2D problem, while still providing the full 3D displacement field.

Previous studies [22, 23, 139] have reported difficulties in maintaining separability when representing distributed loads or solving nonlinear problems, such as material plasticity. In these cases, a large number of modes may be required to achieve accurate results [143]. For instance, Cueto et al. [23] and Zou et al. [139] limited their analyses to moving unit loads to prevent the introduction of too many non-separable parameters in the PGD formulation. Vitse et al. [144] and Néron et al. [145] addressed solving transient nonlinear problems using a hybrid PGD-LATIN approach. The LATIN method, originally proposed by Ladevèze [146–149], acts as an iterative strategy for solving nonlinear problems. When combined with PGD, the separated representation is embedded within the LATIN framework, enabling reduced dimensionality and improved computational efficiency.

In the present work, the decomposition of the problem shown in Section 4.3 is particularly advantageous, as it preserves separability. Instead of solving a coupled nonlinear problem, the elastic (4.4a) and plastic (4.4b) contributions can be computed independently as linear problems using the PGD domain decomposition in (4.7).

In addition to the domain decomposition, the distributed surface load $\boldsymbol{p}$ used to compute $\boldsymbol{u}^{\mathrm{e}}$ in (4.4a) is parameterized within the PGD framework by introducing it as additional coordinates. The semi-Hertzian STRIPES contact model [49, 50] enables this parameterization while preserving separability, as it provides a semi-discrete representation of the contact pressure distribution. Taking advantage of the linearity of the elastic problem, each strip $m = [1, \ldots, M]$ in each loading direction β, can be treated as a separate

problem $\boldsymbol{u}_\beta^m(\boldsymbol{y}, x, b^m)$, where the out-of-plane width b^m of each strip (see Figure 3.2b) is introduced as an additional coordinate alongside the domain decomposition. The total displacement field can then be expressed as a superposition of these solutions

$$\boldsymbol{u}^{\mathrm{e}}(\boldsymbol{y}, x, \boldsymbol{p}) = \sum_{m=1}^{M} \sum_{\beta \in \mathbb{A}} \boldsymbol{u}_\beta^m(\boldsymbol{y}, x, b^m) p_\beta^m, \tag{4.8}$$

where p_β^m denotes the maximum contact traction for each strip and loading direction. The direction indices $\mathbb{A} = \{n, t, x\}$ corresponds to the normal n, lateral l, and longitudinal x direction, respectively. Each $\boldsymbol{u}_\beta^m(\boldsymbol{y}, x, b^m)$ can be approximated using PGD.

For solving $\boldsymbol{u}^{\mathrm{e}}$ in (4.4a), an offline–online separation is used. All modes are computed in the offline phase, enabling near-instantaneous evaluation of particular load cases in the online phase. For $\boldsymbol{u}^{\mathrm{p}}$ in (4.4a), the domain decomposition in (4.7) is used directly in the online stage, since precomputing all possible plastic strain combinations would be infeasible. Nevertheless, the computational cost remains substantially lower than full 3D analysis because the domain decomposition reduces the problem dimensionality.

5. Summary of appended papers

This chapter summarizes the appended papers, which together contribute to the goal of developing digital twins for predicting long-term railhead damage. **Paper A**-**Paper C** lay the foundation by linking field measurements with simulations through data analysis and model calibration. **Paper D**-**Paper E** extend the framework through the development of a ROM that enables efficient 3D simulations of railhead plasticity.

Paper A

Paper A contributes to the development of digital twins by presenting and validating a numerical methodology for predicting long-term railhead damage in curves. This methodology combines field data with simulations of wear, plasticity, and RCF crack initiation under operational traffic conditions. The study focuses on the railhead degradation of the high railhead cross-section in a circular curve. The study utilizes railhead profile data to both calibrate the numerical model and to validate its predictive capability.

The simulation framework includes multiple steps applied in repetition: MBD simulations are utilized to evaluate vehicle-track interaction for a given loading situation and rail profile. This is followed by elasto-plastic wheel–rail contact analysis and damage evaluation in terms of cyclic plastic deformation, surface wear, and surface-initiated RCF. After each cycle, the rail profile is updated from the accumulated wear and plasticity and fed back into the next cycle. To ensure computational efficiency, a metamodel is used for the elasto-plastic contact problem, cyclic plasticity is evaluated through simplified nonlinear 2D FE simulations assuming plane strain, and load collectives are repeated and partly extrapolated in plasticity simulations to reduce the runtime.

The results demonstrate that the model can predict RCF crack initiation and reproduce the average profile changes observed in the field when calibrated with respect to a global wear coefficient and the material yield limit. Figure 5.1 compares measured and simulated profile changes after approximately 10 MGT of traffic, showing the relative contributions from wear and plasticity. The simulations show that wear is the primary driver of long-term profile evolution, while plastic deformation contributes less to the geometry change but can be utilized for predicting RCF crack initiation. In addition, there are some discrepancies between simulated and measured profile changes, particularly near the gauge corner. This can stem from several factors. Firstly, the limited traffic between measurements, therefore, the data is sensitive to measurement errors and the rail alignment. Secondly, simplifications from the Hertzian contact and traffic load representation. Finally, the use of globally calibrated wear and plasticity parameters may not capture local variations along the rail profile.

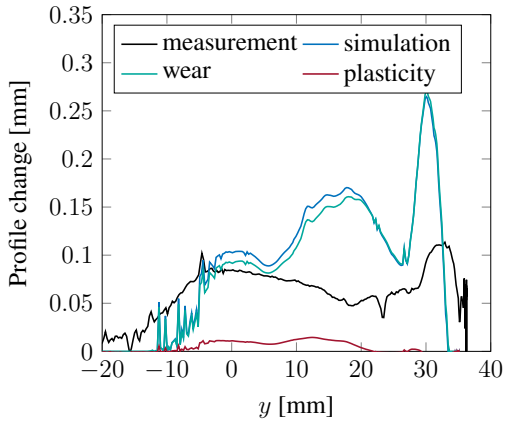

Figure 5.1: *Comparison between measured and simulated profile change in the normal direction for one cross-section after approximately 10 MGT of traffic. The simulation results are calibrated, and the figure illustrates the relative contributions from wear and plastic deformation to the total profile change.*

Paper B

Paper B extends the work in **Paper A** by analyzing how different model parameters influence the wear distribution on a railhead cross-section in a curved track, since there was a discrepancy between the measurement and simulation in **Paper A**. With the overarching goal to improve the predictive ability of the numerical model, this study aimed to identify which parameters of the vehicle and track, as well as the contact model used in the MBD simulations, most strongly affect the contact conditions and thus the resulting wear.

The numerical method builds on the framework established in **Paper A**, combining MBD vehicle-track simulations with Archard's wear law [150] and the FASTSIM [51] discretization of the contact patch. In this study, the railhead geometry is kept fixed, and one model parameter is varied at a time to isolate its effect on the predicted wear distribution. The parameters investigated include vehicle types (passenger versus freight), sets of measured wheel profiles, vehicle suspension stiffness, equilibrium cant, lateral acceleration limits, and the choice of contact model for the normal contact problem. For the latter, both the Hertzian formulation and the semi-Hertzian STRIPES method were considered, the latter allowing for (simplified) elasto-plastic material behavior in the contact.

The parametric study indicates that no single factor drastically alters the predicted wear distribution, suggesting that the original load collective used in **Paper A** already captures the dominant features of the contact conditions. However, three parameters were identified as particularly influential: (1) the inclusion of freight vehicles in the traffic mix, (2) the use of varied measured wheel profiles, and (3) the adoption of the semi-Hertzian contact model. Each of these factors broadened the simulated wear distribution across the

railhead, resulting in a closer resemblance to the field measurements. Other parameters, such as cant or increased suspension stiffness, mainly affected the magnitude of wear rather than its distribution.

Paper C

Paper C extends the work of **Paper A** and **Paper B** by advancing the digital twin framework for long-term railhead damage prediction in curves. The study combines field measurements with the same numerical method as in **Paper A**, focusing on wear and incorporating a semi-Hertzian contact model based on the results from **Paper B**. In addition, it applies and extends the parametric analysis for the load collective from **Paper B** to better represent the operational traffic.

In this study, eight field measurement occasions are available, capturing the gradual material removal from wear and grinding over time. These measurements provide a more detailed basis for validating the simulations. The accuracy of the predictions is improved through an enhanced calibration procedure. Instead of relying on a single global wear coefficient as in **Paper A**, the key coefficients in Jendel's wear map [81] are identified and calibrated. Since optimizing multiple coefficients would require many full simulations, surrogate modeling combined with an optimization algorithm is used to efficiently explore the parameter space. Latin Hypercube Sampling (LHS) [106] is used to generate training data, from which surrogate functions are built to approximate the simulation response. The appropriate simulation length (amount of traffic) and sample size are determined to ensure reliable training data.

The enhanced calibration procedure significantly increases predictive accuracy compared to **Paper A**, as reflected in the improved match between simulated and measured profile change seen in Figure 5.2. The agreement is particularly strong at 10 MGT of traffic, probably because the measurement data was used in the calibration. The model also predicts the data for 20 MGT of traffic well, although that data was not used in the calibration. This indicates that the calibrated parameters generalize well to higher traffic volumes. Some discrepancies remain, such as the overestimated wear at the rail top, but these are acceptable given the uncertainties associated with long-term damage prediction. These uncertainties arise from unknown variations in traffic conditions, simplifications in the modeling assumptions, and the limited accuracy of the measurement data itself. This is evident upon comparing the relatively small discrepancies to the rather large variation in measurements at different instances along the curved section shown in Figure 2.6. Overall, the calibration of the wear map yields a wear distribution that aligns more closely with field data compared to **Paper A**. The proposed surrogate-based optimization ensures computational efficiency, making the approach suitable for integration into a digital twin framework.

Paper D

Paper D takes a first step towards developing a ROM for efficiently predicting evolving railhead plasticity. The model focuses on the 3D elastic response of a railhead subjected

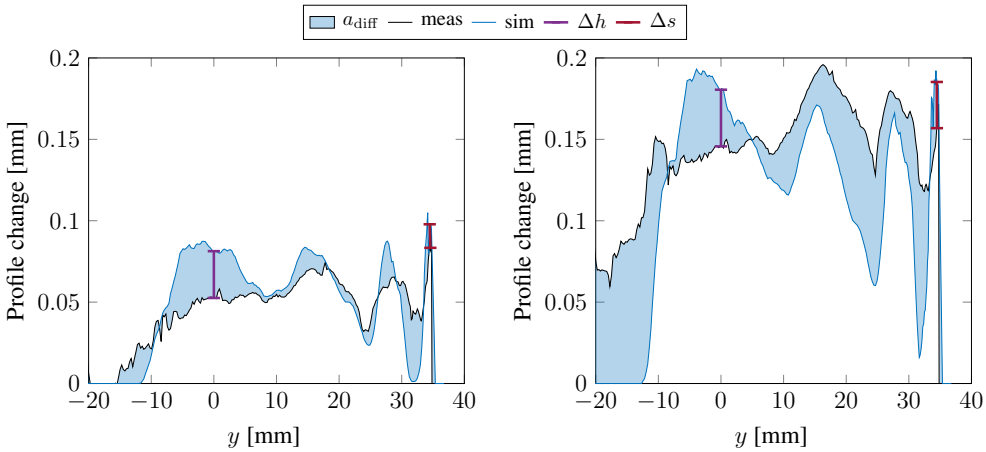

***(a)** 10 MGT* *(b) 20 MGT*

Figure 5.2: *Profile change for the optimized parameter set compared to measurements, gauge corner to the right, at (a) 10 MGT and (b) 20 MGT. The shaded areas indicate the difference between simulation and measurement a_{diff}, while Δh and Δs illustrate the vertical and horizontal differences.*

to different contact scenarios. The study introduces a ROM framework based on the PGD technique to retain the accuracy of a 3D simulation at almost 2D computational effort.

The methodology includes a domain decomposition of the 3D solid railhead, wherein a 2D in-plane cross-section and a one-dimensional out-of-plane discretization are treated as parameters in the PGD approximation. This separation reduces the full 3D problem to 2D and 1D problems, thereby ensuring that the computational cost scales with the 2D calculations while still capturing the fully resolved 3D stress state.

To account for different load scenarios in an efficient manner, the PGD framework is extended by incorporating the semi-Hertzian STRIPES [49, 50] approach. STRIPES is chosen since it showed promising results in **Paper B**. Furthermore, in comparison to Hertzian contact, it provides greater separability and allows multiple simultaneous contact points. The contact load is parameterized so that it can be included as additional coordinates in the PGD formulation. In the implementation, the linearity of the elastic problem is exploited by treating each strip in each loading direction as a separate PGD expansion, with the out-of-plane width of the contact strip being incorporated as an additional coordinate alongside the domain decomposition.

The proposed framework demonstrates high accuracy in predicting the 3D elastic response of the railhead under various contact load scenarios using PGD, while maintaining a computational complexity comparable to that of 2D simulations. This efficiency is demonstrated in Figure 5.3, which compares the PGD solution with conventional 3D FE analysis. The figures show significant reductions in CPU time and memory usage, while achieving similar accuracy in displacements and stresses. Once the PGD solution has been constructed offline for a wide range of load distributions, new contact scenarios can

be evaluated almost instantly in the online phase by superimposing precomputed PGD solutions. This facilitates efficient simulations across many load cases, thereby establishing a foundation for extending the framework to elasto-plastic material behavior, as pursued in **Paper E**.

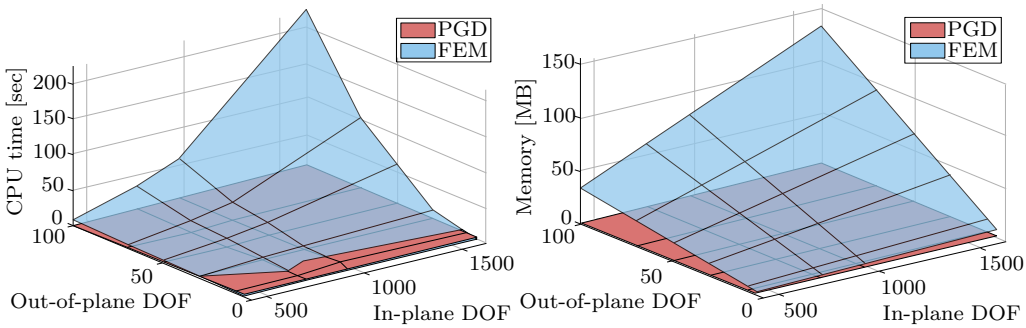

Figure 5.3: *Comparisons of (a) CPU time and (b) memory usage between PGD and conventional 3D FE simulations for different in-plane and out-of-plane discretizations.*

Paper E

Paper E builds upon the work done in **Paper D** and presents a ROM framework to efficiently predict evolving plasticity in a 3D railhead subjected to many wheel–rail overrollings. This study aims to enhance the accuracy of earlier 2D FE elasto-plastic simulations by switching to a 3D representation of the railhead, while maintaining computational efficiency. This is imperative for integration into a digital twin framework, wherein simulations must be both accurate and rapid to support long-term predictions of railhead damage.

The methodology extends the PGD-based formulation introduced in **Paper D** to incorporate elasto-plastic material behavior. The approach is structured around three main components. First, under the assumption of steady-state conditions, a convective coordinate system that follows the contact along the railhead is introduced. This transforms the moving load into a stationary contact problem, making the material response time-independent. The response can then be tracked along streamlines in the spatial mesh, which enables parallelization across integration points in the railhead cross-section and thereby accelerates the computation of plastic strain. Second, an iterative fixed-point scheme is implemented to address the coupling between the displacement field and the plastic strains. Third, the PGD framework with domain decomposition, as presented in **Paper D**, is used to efficiently solve the 3D displacement field. Upon achieving convergence, the process is repeated for subsequent overrollings.

Validation against full 3D FE simulations for different Hertzian contact load scenarios shows that the ROM captures the displacement field for both a single overrolling and

for multiple overrollings with high accuracy, as illustrated in Figure 5.4. It has been demonstrated that convergence is achieved within only a few fixed-point iterations per overrolling, resulting in a substantial increase in efficiency, estimated to be 63 times faster than reference simulations. This efficiency is crucial for simulating accumulated plastic deformation over many wheel passages, which would be computationally prohibitive with conventional 3D FE models.

Beyond these results, the ROM framework offers a promising basis for integration into a digital twin, where rapid yet accurate simulations are essential. Due to the fully resolved 3D stress and strain states, the simulations allow predicting the initiation and orientation of RCF cracks in the future extension of the digital twin.

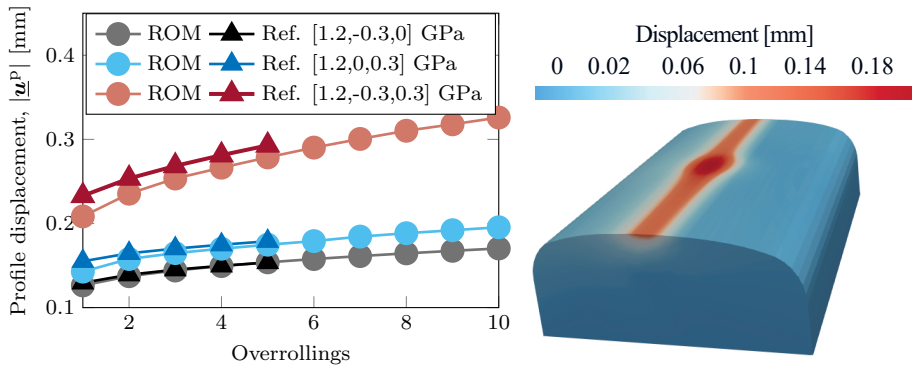

(a) *(b)*

Figure 5.4: *Displacement field for multiple overrollings. (a) Norm of nodal displacement vector of the permanent profile after each overrolling for the ROM and reference solution. Norm of displacement field in the ROM solution after five overrollings.*

6. Conclusions and outlook

The overall goal of this thesis was to develop computationally efficient digital twins capable of predicting long-term railhead damage in curved railway sections under operational traffic conditions. To achieve this, the work was structured around two main objectives. First, to develop and calibrate a numerical model for use in a digital twin framework. Second, to improve computational efficiency through Reduced Order Modeling (ROM). The appended papers collectively contribute to fulfilling these objectives and demonstrate the potential of digital twins as data-informed decision support tools for railway maintenance.

Regarding the first objective, **Paper A**-**Paper C** established a numerical framework for predicting long-term railhead damage. The framework combines MBD vehicle-track simulations and railhead damage evolution, accounting for wear, plastic deformation, and Rolling Contact Fatigue (RCF) initiation. The predictive accuracy of the model was improved by calibrating against field data of railhead profiles. **Paper A** formulated the workflow and demonstrated that, when calibrated with global parameters for the wear coefficient and the material yield limit, the model can reproduce the average changes in the geometry of the railhead. In **Paper B**, the influence of modeling choices related to the formulation of the contact or parameters related to the track or vehicle was highlighted. The findings indicated that adopting a semi-Hertzian contact model, using a different set of measured wheel profiles, or including freight vehicles in the traffic scenario resulted in improved prediction of the profile change distribution. **Paper C** introduced a refined calibration procedure by combining surrogate modeling and optimization to efficiently find optimal wear coefficients in Jendel's wear map. This approach improved the agreement with the measured profile change distribution. It is noteworthy that the calibrated parameters demonstrated a high degree of generalization, extending beyond the calibration interval to higher traffic levels. This verifies the model's capability for reliable railhead damage predictions. The collective contributions from these papers demonstrate how continuous updates with measurements and systematic model calibration strengthen the link between simulation and field data, thereby enhancing the predictive capability required in a digital twin framework.

The second objective was addressed in **Paper D**-**Paper E**, where ROMs based on the Proper Generalized Decomposition (PGD) method were developed. In **Paper D**, a PGD formulation with domain decomposition and parametrized distributed contact load was introduced to compute the 3D elastic response of the railhead under different contact load scenarios. This approach yields a computational cost that is nearly equivalent to that of a 2D model while maintaining the accuracy of a full 3D model. The framework was extended in **Paper E** to account for elasto-plastic material, allowing efficient computation of the evolution of plasticity for many passages of the wheel. The approach is comprised of three distinct components. First, the transformation of the moving-load problem into a

stationary problem is achieved by using a convective coordinate system under steady-state assumptions. Secondly, the coupling between the displacement field and the plastic strains is addressed by using an iterative scheme. Thirdly, the PGD framework developed in **Paper D** is used to effectively solve the displacement field. The ROM was validated against full 3D finite element simulations, which demonstrated substantial speedups while maintaining high accuracy. These results demonstrate the ROMs capability to provide the computational efficiency required for long-term damage predictions in digital twin simulations.

At the same time, several challenges persist that present opportunities for future research. To enhance the accuracy of long-term predictions, there is a need for improved field data, including systematic information on cracks, precise records of material removed during grinding, and more detailed descriptions of operational conditions. The ROM framework should be implemented in the digital twin framework presented in **Paper A**-**Paper C** to more accurately capture the evolution of plasticity in rails. In addition, it can also be combined with an RCF criterion to enhance the predictive ability of crack initiation and its direction, particularly now that the full multiaxial stress-strain history is predicted. Furthermore, the current work is limited to the contact models available in either the MBD simulation software or the Hertzian-inspired metamodel. For the ROM proposed in **Paper Paper E**, and for all simulations of wear in **Paper Paper A**-**Paper Paper C**, contact stresses are obtained directly for the contact models in the MBD simulations, which do not account for inelastic response in the contact patch. Consequently, there is a need for more accurate contact models that can account for inelastic material responses, particularly in the tangential direction. One possible development would be to extend the ROM so that it can serve as a contact model within an MBD simulation framework, enabling computationally efficient analyses while capturing detailed geometric and material effects.

6. References

[1] B. Åkesson. *SIKAs data och ökad säkerhet for persontransporter*. Tech. rep. Jan. 2010, p. 3.

[2] C. Doll et al. *Methodology for GHG Efficiency of Transport Modes*. Tech. rep. 2020, p. 88.

[3] International Energy Agency. *The Future of Rail: Opportunities for energy and the environment*. OECD, Feb. 2019. ISBN: 978-92-64-31282-1. DOI: 10.1787/9789264312821-en.

[4] D. F. Cannon and H. Pradier. "Rail rolling contact fatigue Research by the European Rail Research Institute". en. In: *Wear*. 4th International Conference on Contact Mechanics and Wear of Rail-Wheel Systems 191.1 (Jan. 1996), pp. 1–13. ISSN: 0043-1648. DOI: 10.1016/0043-1648(95)06650-0.

[5] A. Kapoor. "A Re-Evaluation of the Life to Rupture of Ductile Metals by Cyclic Plastic Strain". In: *Fatigue & Fracture of Engineering Materials & Structures* 17.2 (1994), pp. 201–219. ISSN: 1460-2695. DOI: 10.1111/j.1460-2695.1994.tb00801.x.

[6] M. Schilke, N. Larijani, and C. Persson. "Interaction between cracks and microstructure in three dimensions for rolling contact fatigue in railway rails". en. In: *Fatigue & Fracture of Engineering Materials & Structures* 37.3 (2014), pp. 280–289. ISSN: 1460-2695. DOI: 10.1111/ffe.12112.

[7] G. Donzella et al. "Progressive damage assessment in the near-surface layer of railway wheel–rail couple under cyclic contact". In: *Wear*. Proceedings of the 8th International Conference on Contact Mechanics and Wear of Rail / Wheel Systems, Florence, 2009 271.1 (May 2011), pp. 408–416. ISSN: 0043-1648. DOI: 10.1016/j.wear.2010.10.042.

[8] A. Smith et al. "Estimating the relative cost of track damage mechanisms: combining economic and engineering approaches". en. In: *Proceedings of the Institution of Mechanical Engineers, Part F: Journal of Rail and Rapid Transit* 231.5 (May 2017). Publisher: IMECHE, pp. 620–636. ISSN: 0954-4097. DOI: 10.1177/0954409717698850.

[9] "The Swedish Transport Administration Annual Report 2017". en. In: *Trafikverket* 2018:086 (2017), pp. 34–37.

[10] W. Schoech, R. Heyder, and H.-D. Grohmann. "Contact geometry and surface fatigue - guidelines for appropriate rail maintenance". en. In: *7th International Conference on Contact Mechanics and Wear of Rail/Wheel Systems (CM2006)*. Brisbane, Australia, Sept. 2006, p. 7.

[11] *Svensk Standard SS-EN 13231-5:2018 - Railway applications – Track – Acceptance of works – Part 5: Procedures for rail reprofiling in plain line, switches, crossings and expansion devices*. sv. 2018.

[12] A. Johansson et al. “Simulation of wheel–rail contact and damage in switches & crossings”. en. In: *Wear*. Proceedings of the 8th International Conference on Contact Mechanics and Wear of Rail / Wheel Systems, Florence, 2009 271.1 (May 2011), pp. 472–481. ISSN: 0043-1648. DOI: 10.1016/j.wear.2010.10.014.

[13] R. Skrypnyk et al. “Long-term rail profile damage in a railway crossing: Field measurements and numerical simulations”. en. In: *Wear* 472-473 (May 2021). ISSN: 0043-1648. DOI: 10.1016/j.wear.2020.203331.

[14] S. Hossein-Nia et al. “Wheel life prediction model – an alternative to the FASTSIM algorithm for RCF”. en. In: *Vehicle System Dynamics* 56.7 (July 2018), pp. 1051–1071. ISSN: 0042-3114, 1744-5159. DOI: 10.1080/00423114.2017.1403636.

[15] V. V. Krishna et al. “Long term rail surface damage considering maintenance interventions”. en. In: *Wear* 460-461 (Nov. 2020). ISSN: 0043-1648. DOI: 10.1016/j.wear.2020.203462.

[16] G. Trummer et al. “Modeling surface rolling contact fatigue crack initiation taking severe plastic shear deformation into account”. en. In: *Wear* 352-353 (Apr. 2016), pp. 136–145. ISSN: 0043-1648. DOI: 10.1016/j.wear.2016.02.008.

[17] K. D. Vo et al. “FE method to predict damage formation on curved track for various worn status of wheel/rail profiles”. en. In: *Wear* 322-323 (Jan. 2015), pp. 61–75. ISSN: 0043-1648. DOI: 10.1016/j.wear.2014.10.015.

[18] A. Rasheed, O. San, and T. Kvamsdal. “Digital Twin: Values, Challenges and Enablers From a Modeling Perspective”. In: *IEEE Access* 8 (2020), pp. 21980–22012. ISSN: 2169-3536. DOI: 10.1109/ACCESS.2020.2970143.

[19] A. Ferrari and K. Willcox. “Digital twins in mechanical and aerospace engineering”. en. In: *Nature Computational Science* 4.3 (Mar. 2024). Publisher: Nature Publishing Group, pp. 178–183. ISSN: 2662-8457. DOI: 10.1038/s43588-024-00613-8.

[20] J. L. Lumley. “The structure of inhomogeneous turbulent flows”. In: *Atmospheric Turbulence and Radio Wave Propagation* (1967). Publisher: Nauka, pp. 166–178.

[21] S. Wold, K. Esbensen, and P. Geladi. “Principal component analysis”. In: *Chemometrics and Intelligent Laboratory Systems*. Proceedings of the Multivariate Statistical Workshop for Geologists and Geochemists 2.1 (Aug. 1987), pp. 37–52. ISSN: 0169-7439. DOI: 10.1016/0169-7439(87)80084-9.

[22] F. Chinesta, R. Keunings, and A. Leygue. *The Proper Generalized Decomposition for Advanced Numerical Simulations*. en. SpringerBriefs in Applied Sciences and Technology. Cham: Springer International Publishing, 2014. DOI: 10.1007/978-3-319-02865-1.

[23] E. Cueto, D. González, and I. Alfaro. *Proper Generalized Decompositions*. en. SpringerBriefs in Applied Sciences and Technology. Cham: Springer International Publishing, 2016.

[24] R. Skrypnyk et al. “Metamodelling of wheel–rail normal contact in railway crossings with elasto-plastic material behaviour”. en. In: *Engineering with Computers* 35.1 (Jan. 2019), pp. 139–155. ISSN: 0177-0667, 1435-5663. DOI: 10.1007/s00366-018-0589-3.

[25] E. Andersson, M. Berg, and S. Stichel. *Rail Vehicle Dynamics*. Swedish. Stockholm: Centre for Research and Education in Railway Engineering, Railway Group KTH, 2007. ISBN: 91-7415-272-6.

[26] A. Kapoor, I. Salehi, and A. M. S. Asih. "Rolling Contact Fatigue (RCF)". en. In: *Encyclopedia of Tribology*. Ed. by Q. J. Wang and Y.-W. Chung. Boston, MA: Springer US, 2013, pp. 2904–2910. ISBN: 978-0-387-92897-5. DOI: 10.1007/978-0-387-92897-5_287.

[27] F. W. Carter and A. E. H. Love. "On the action of a locomotive driving wheel". In: *Proceedings of the Royal Society of London. Series A, Containing Papers of a Mathematical and Physical Character* 112.760 (1926). Publisher: Royal Society, pp. 151–157. DOI: 10.1098/rspa.1926.0100.

[28] H. Fromm. "Berechnung des Schlupfes beim Rollen deformierbarer Scheiben". en. In: *ZAMM - Journal of Applied Mathematics and Mechanics* 7.1 (1927), pp. 27–58. ISSN: 1521-4001. DOI: 10.1002/zamm.19270070106.

[29] A. Ekberg and E. Kabo. "Key parameters and requirements for track health prediction". en. In: (), p. 71.

[30] R. Deuce, A. Ekberg, and E. Kabo. "Mechanical deterioration of wheels and rails under winter conditions – mechanisms and consequences". EN. In: *Proceedings of the Institution of Mechanical Engineers, Part F: Journal of Rail and Rapid Transit* 233.6 (July 2019). Publisher: IMECHE, pp. 640–648. ISSN: 0954-4097. DOI: 10.1177/0954409718802437.

[31] A. Ekberg and E. Kabo. "Fatigue of railway wheels and rails under rolling contact and thermal loading—an overview". In: *Wear*. Contact Mechanics and Wear of Rail/Wheel Systems 258.7 (Mar. 2005), pp. 1288–1300. ISSN: 0043-1648. DOI: 10.1016/j.wear.2004.03.039.

[32] K. A. Meyer, D. Nikas, and J. Ahlström. "Microstructure and mechanical properties of the running band in a pearlitic rail steel: Comparison between biaxially deformed steel and field samples". en. In: *Wear* 396-397 (Feb. 2018), pp. 12–21. ISSN: 0043-1648. DOI: 10.1016/j.wear.2017.11.003.

[33] K. Karttunen. "Influence of rail, wheel and track geometries on wheel and rail degradation". en. In: (2012).

[34] B. Dirks. "Simulation and measurement of wheel on rail fatigue and wear". en. In: (Apr. 2015). ISSN: 1651-766.

[35] U. Olofsson and T. Telliskivi. "Wear, plastic deformation and friction of two rail steels—a full-scale test and a laboratory study". en. In: *Wear* 254.1 (Jan. 2003), pp. 80–93. ISSN: 0043-1648. DOI: 10.1016/S0043-1648(02)00291-0.

[36] Y. Zhou et al. "Field and laboratory investigation of the relationship between rail head check and wear in a heavy-haul railway". In: *Wear* 315.1 (July 2014), pp. 68–77. ISSN: 0043-1648. DOI: 10.1016/j.wear.2014.04.004.

[37] A. Ekberg and P. Sotkovszki. "Anisotropy and rolling contact fatigue of railway wheels". en. In: *International Journal of Fatigue* 23.1 (Jan. 2001), pp. 29–43. ISSN: 0142-1123. DOI: 10.1016/S0142-1123(00)00070-0.

[38] W. J. Wang et al. "Investigation on the damage mechanism and prevention of heavy-haul railway rail". en. In: *Engineering Failure Analysis*. Special issue on ICEFA V- Part 1 35 (Dec. 2013), pp. 206–218. ISSN: 1350-6307. DOI: 10.1016/j.engfailanal.2013.01.033.

[39] N. Larijani et al. "The effect of anisotropy on crack propagation in pearlitic rail steel". en. In: *Wear*. Proceedings of the 9th International Conference on Contact

Mechanics and Wear of Rail / Wheel Systems, Chengdu, 2012 314.1 (June 2014), pp. 57–68. ISSN: 0043-1648. DOI: 10.1016/j.wear.2013.11.034.

[40] R. Lewis et al. "Mapping railway wheel material wear mechanisms and transitions". EN. In: *Proceedings of the Institution of Mechanical Engineers, Part F: Journal of Rail and Rapid Transit* 224.3 (May 2010). Publisher: IMECHE, pp. 125–137. ISSN: 0954-4097. DOI: 10.1243/09544097JRRT328.

[41] *MiniProf - Digital Profile Measuring*. en-US.

[42] *MiniProf Envision*. 2022.

[43] *Spårkomponenter: TRVINFRA-00018 Krav Version 6.0*. Jan. 2025.

[44] R. Skrypnyk et al. "Prediction of plastic deformation and wear in railway crossings – Comparing the performance of two rail steel grades". en. In: *Wear* 428-429 (June 2019), pp. 302–314. ISSN: 0043-1648. DOI: 10.1016/j.wear.2019.03.019.

[45] R. Skrypnyk et al. "On the influence of crossing angle on long-term rail damage evolution in railway crossings". In: *International Journal of Rail Transportation* 9.6 (Jan. 2021), pp. 503–519. ISSN: 2324-8378. DOI: 10.1080/23248378.2020.1864794.

[46] *The GENSYS Homepage*.

[47] SIMPACK. *Simpack Multibody System Simulation Software*. en.

[48] H. Hertz. "On the contact of solid, elastic bodies". In: *Journal für die reine und angewandte Mathematik* 92 (1882), pp. 156–171.

[49] J. Ayasse and H. Chollet. "Determination of the wheel rail contact patch in semi-Hertzian conditions". In: *Vehicle System Dynamics* 43.3 (Mar. 2005), pp. 161–172. ISSN: 0042-3114. DOI: 10.1080/00423110412331327193.

[50] X. Quost et al. "Assessment of a semi-Hertzian method for determination of wheel–rail contact patch". In: *Vehicle System Dynamics* 44.10 (Oct. 2006), pp. 789–814. ISSN: 0042-3114. DOI: 10.1080/00423110600677948.

[51] J. Kalker. "A Fast Algorithm for the Simplified Theory of Rolling Contact". In: *Vehicle System Dynamics* 11.1 (Feb. 1982), pp. 1–13. ISSN: 0042-3114. DOI: 10.1080/00423118208968684.

[52] J. J. Kalker. *Three-Dimensional Elastic Bodies in Rolling Contact*. en. Springer Science & Business Media, Oct. 1990. ISBN: 978-0-7923-0712-9.

[53] J. J. Kalker. "Wheel-rail rolling contact theory". en. In: *Wear* 144.1 (Apr. 1991), pp. 243–261. ISSN: 0043-1648. DOI: 10.1016/0043-1648(91)90018-P.

[54] K. L. Johnson. *Contact Mechanics*. en. Cambridge University Press, Aug. 1987. ISBN: 978-0-521-34796-9.

[55] S. Z. Meymand, A. Keylin, and M. Ahmadian. "A survey of wheel–rail contact models for rail vehicles". In: *Vehicle System Dynamics* 54.3 (Mar. 2016). Publisher: Taylor & Francis _eprint: https://doi.org/10.1080/00423114.2015.1137956, pp. 386–428. ISSN: 0042-3114. DOI: 10.1080/00423114.2015.1137956.

[56] M. Sebès et al. "A fast-simplified wheel–rail contact model consistent with perfect plastic materials". In: *Vehicle System Dynamics* 50.9 (Sept. 2012), pp. 1453–1471. ISSN: 0042-3114. DOI: 10.1080/00423114.2012.669483.

[57] L. Chevalier et al. "Taking into account plasticity in real time wheel-rail contact model". In: *9th International Conference on Contact Mechanic and Wear of Rail/Wheel Systems*. Chengdu, China, 2012.

[58] J. J. Kalker. “Survey of Wheel—Rail Rolling Contact Theory”. en. In: *Vehicle System Dynamics* 8.4 (Sept. 1979), pp. 317–358. ISSN: 0042-3114, 1744-5159. DOI: 10.1080/00423117908968610.

[59] K. Zaazaa and A. Schwab. “Review of Joost Kalker’s Wheel-Rail Contact Theories and Their Implementation in Multibody Codes”. In: Jan. 2009. DOI: 10.1115/DETC2009-87655.

[60] J. J. Kalker. “Review of wheel-rail rolling contact theories”. en-US. In: *Publication of: American Society of Mechanical Engineers* (1980).

[61] M. Shahzamanian Sichani. *On Efficient Modelling of Wheel-Rail Contact in Vehicle Dynamics Simulation*. en. Stockholm: KTH Royal Institute of Technology, 2016. ISBN: 978-91-7595-846-0.

[62] M. Pletz et al. “Cyclic plastic deformation of rails in rolling/sliding contact –quasistatic FE calculations using different plasticity models”. In: *Wear* 436-437 (Oct. 2019), p. 202992. ISSN: 0043-1648. DOI: 10.1016/j.wear.2019.202992.

[63] K. A. Meyer, R. Skrypnyk, and M. Pletz. “Efficient 3d finite element modeling of cyclic elasto-plastic rolling contact”. In: *Tribology International* 161 (Sept. 2021), p. 107053. ISSN: 0301-679X. DOI: 10.1016/j.triboint.2021.107053.

[64] J. Zhao et al. “Numerical investigation on the rolling contact wear and fatigue of laser dispersed quenched U71Mn rail”. In: *International Journal of Fatigue* 143 (Feb. 2021), p. 106010. ISSN: 0142-1123. DOI: 10.1016/j.ijfatigue.2020.106010.

[65] Z. Zhou et al. “Three-dimensional elastic–plastic stress analysis of wheel–rail cyclic rolling contact using finite element method”. In: *Wear* 542-543 (Apr. 2024), p. 205277. ISSN: 0043-1648. DOI: 10.1016/j.wear.2024.205277.

[66] J. P. Srivastava et al. “Rolling Contact Fatigue Life of Rail for Different Slip Conditions”. en. In: *Latin American Journal of Solids and Structures* 14 (Dec. 2017), pp. 2243–2264. ISSN: 1679-7817, 1679-7825. DOI: 10.1590/1679-78254161.

[67] Z. Wen, X. Jin, and Y. Jiang. “Elastic-Plastic Finite Element Analysis of Nonsteady State Partial Slip Wheel-Rail Rolling Contact”. In: *Journal of Tribology* 127.4 (June 2005), pp. 713–721. ISSN: 0742-4787. DOI: 10.1115/1.2033898.

[68] B. Andersson, M. Ekh, and B. L. Josefson. “Computationally efficient simulation methodology for railway repair welding: Cyclic plasticity, phase transformations and multi-phase homogenization”. In: *Journal of Thermal Stresses* 47.2 (Feb. 2024). Publisher: Taylor & Francis _eprint: https://doi.org/10.1080/01495739.2023.2283309, pp. 164–188. ISSN: 0149-5739. DOI: 10.1080/01495739.2023.2283309.

[69] N. Talebi et al. “Influence of a highly deformed surface layer on RCF predictions for rails in service”. In: *Wear* 578-579 (Sept. 2025), p. 206173. ISSN: 0043-1648. DOI: 10.1016/j.wear.2025.206173.

[70] G. Johansson and M. Ekh. “On the modeling of large ratcheting strains with large time increments”. In: *Engineering Computations* 24.3 (Jan. 2007). Publisher: Emerald Group Publishing Limited, pp. 221–236. ISSN: 0264-4401. DOI: 10.1108/02644400710734945.

[71] S. Bari and T. Hassan. “Anatomy of coupled constitutive models for ratcheting simulation”. In: *International Journal of Plasticity* 16.3 (Jan. 2000), pp. 381–409. ISSN: 0749-6419. DOI: 10.1016/S0749-6419(99)00059-5.

[72] J. L. Chaboche. “A review of some plasticity and viscoplasticity constitutive theories”. In: *International Journal of Plasticity*. Special Issue in Honor of Jean-Louis Chaboche 24.10 (Oct. 2008), pp. 1642–1693. ISSN: 0749-6419. DOI: 10.1016/j.ijplas.2008.03.009.

[73] N. Ohno and J.-D. Wang. “Kinematic hardening rules with critical state of dynamic recovery, part I: formulation and basic features for ratchetting behavior”. en. In: *International Journal of Plasticity* 9.3 (Jan. 1993), pp. 375–390. ISSN: 0749-6419. DOI: 10.1016/0749-6419(93)90042-O.

[74] R. Brommesson, M. Ekh, and M. Hörnqvist. “Correlation between crack length and load drop for low-cycle fatigue crack growth in Ti-6242”. en. In: *International Journal of Fatigue* 81 (Dec. 2015), pp. 1–9. ISSN: 0142-1123. DOI: 10.1016/j.ijfatigue.2015.07.006.

[75] J. Ahlström and B. Karlsson. “Fatigue behaviour of rail steel—a comparison between strain and stress controlled loading”. en. In: *Wear*. Contact Mechanics and Wear of Rail/Wheel Systems 258.7 (Mar. 2005), pp. 1187–1193. ISSN: 0043-1648. DOI: 10.1016/j.wear.2004.03.030.

[76] J. F. Archard. “Contact and Rubbing of Flat Surfaces”. In: *Journal of Applied Physics* 24.8 (Aug. 1953). Publisher: American Institute of Physics, pp. 981–988. ISSN: 0021-8979. DOI: 10.1063/1.1721448.

[77] J. De Arizon, O. Verlinden, and P. Dehombreux. “Prediction of wheel wear in urban railway transport: comparison of existing models”. In: *Vehicle System Dynamics* 45.9 (Sept. 2007), pp. 849–866. ISSN: 0042-3114. DOI: 10.1080/00423110601149335.

[78] I. McEwen and R. Harvey. “Full-scale wheel-on-rail wear testing: comparisons with service wear and a developing theoretical predictive method”. In: *ASLE/ASME Lubrication Conference* (1983).

[79] T. G. Pearce and N. D. Sherratt. “Prediction of wheel profile wear”. In: *Wear* 144.1 (Apr. 1991), pp. 343–351. ISSN: 0043-1648. DOI: 10.1016/0043-1648(91)90025-P.

[80] I. Zobory. “Prediction of Wheel/Rail Profile Wear”. In: *Vehicle System Dynamics* 28.2-3 (Aug. 1997), pp. 221–259. ISSN: 0042-3114. DOI: 10.1080/00423119708969355.

[81] T. Jendel. “Prediction of wheel profile wear—comparisons with field measurements”. en. In: *Wear*. CM2000 S.I. 253.1 (July 2002), pp. 89–99. ISSN: 0043-1648. DOI: 10.1016/S0043-1648(02)00087-X.

[82] D. Y. Li and H. Pan. “A wearing energy model”. In: *Journal of Applied Physics* 128.19 (Nov. 2020), p. 195105. ISSN: 0021-8979. DOI: 10.1063/5.0024491.

[83] R. Enblom and M. Berg. “Proposed procedure and trial simulation of rail profile evolution due to uniform wear”. EN. In: *Proceedings of the Institution of Mechanical Engineers, Part F* 222.1 (Jan. 2008). Publisher: IMECHE, pp. 15–25. ISSN: 0954-4097. DOI: 10.1243/09544097JRRT173.

[84] J. Brouzoulis et al. “Prediction of wear and plastic flow in rails—Test rig results, model calibration and numerical prediction”. en. In: *Wear*. Proceedings of the 8th International Conference on Contact Mechanics and Wear of Rail / Wheel Systems, Florence, 2009 271.1 (May 2011), pp. 92–99. ISSN: 0043-1648. DOI: 10.1016/j.wear.2010.10.021.

[85] C. Chang et al. “A Study of a Numerical Analysis Method for the Wheel-Rail Wear of a Heavy-Haul Train”. en. In: *Proceedings of the Institution of Mechanical Engineers, Part F: Journal of Rail and Rapid Transit* 224.5 (Sept. 2010), pp. 473–482. ISSN: 0954-4097. DOI: 10.1243/09544097JRRT341.

[86] J. C. O. Nielsen, B. A. Pålsson, and P. T. Torstensson. “Switch panel design based on simulation of accumulated rail damage in a railway turnout”. en. In: *Wear*. Contact Mechanics and Wear of Rail / Wheel Systems, CM2015, August 2015 366-367 (Nov. 2016), pp. 241–248. ISSN: 0043-1648. DOI: 10.1016/j.wear.2016.06.021.

[87] R. Heyder and M. Brehmer. “Empirical studies of head check propagation on the DB network”. In: *Wear*. Proceedings of the 9th International Conference on Contact Mechanics and Wear of Rail / Wheel Systems, Chengdu, 2012 314.1 (June 2014), pp. 36–43. ISSN: 0043-1648. DOI: 10.1016/j.wear.2013.11.035.

[88] J. W. Ringsberg. “Life prediction of rolling contact fatigue crack initiation”. In: *International Journal of Fatigue* 23.7 (Aug. 2001), pp. 575–586. ISSN: 0142-1123. DOI: 10.1016/S0142-1123(01)00024-X.

[89] F. Sadeghi et al. “A Review of Rolling Contact Fatigue”. In: *Journal of Tribology* 131.041403 (Sept. 2009). ISSN: 0742-4787. DOI: 10.1115/1.3209132.

[90] F. J. Franklin and A. Kapoor. “Modelling wear and crack initiation in rails”. EN. In: *Proceedings of the Institution of Mechanical Engineers, Part F: Journal of Rail and Rapid Transit* 221.1 (Jan. 2007). Publisher: IMECHE, pp. 23–33. ISSN: 0954-4097. DOI: 10.1243/0954409JRRT60.

[91] M. C. Burstow. “Whole Life Rail Model Application and Development for RSSB – Continued Development of an RCF Damage Parameter”. en. In: *Rail Standards and Safety Board, London* 2 (2004), p. 74.

[92] K. Golos and F. Ellyin. “A Total Strain Energy Density Theory for Cumulative Fatigue Damage”. In: *Journal of Pressure Vessel Technology* 110.1 (Feb. 1988), pp. 36–41. ISSN: 0094-9930. DOI: 10.1115/1.3265565.

[93] F. J. Franklin et al. “Modelling rail steel microstructure and its effect on crack initiation”. In: *Wear*. Contact Mechanics and Wear of Rail/Wheel Systems - CM2006 265.9 (Oct. 2008), pp. 1332–1341. ISSN: 0043-1648. DOI: 10.1016/j.wear.2008.03.027.

[94] M. Ghodrati, M. Ahmadian, and R. Mirzaeifar. “Modeling of rolling contact fatigue in rails at the microstructural level”. In: *Wear* 406-407 (July 2018), pp. 205–217. ISSN: 0043-1648. DOI: 10.1016/j.wear.2018.04.016.

[95] K. Johnson. “The strength of surfaces in rolling contact”. English. In: *Proceedings of the Institution of Mechanical Engineers, Part C: Journal of Mechanical Engineering Science* 203.3 (May 1989), pp. 151–163. ISSN: 0954-4062. DOI: 10.1243/PIME_PROC_1989_203_100_02.

[96] A. R. S. Ponter, A. D. Hearle, and K. L. Johnson. “Application of the kinematical shakedown theorem to rolling and sliding point contacts”. en. In: *Journal of the Mechanics and Physics of Solids* 33.4 (Jan. 1985), pp. 339–362. ISSN: 0022-5096. DOI: 10.1016/0022-5096(85)90033-X.

[97] A. Ekberg, E. Kabo, and H. Andersson. “An engineering model for prediction of rolling contact fatigue of railway wheels”. en. In: *Fatigue & Fracture of Engineering*

Materials & Structures 25.10 (2002), pp. 899–909. ISSN: 1460-2695. DOI: 10.1046/j.1460-2695.2002.00535.x.

[98] K. Dang Van. "On a new multiaxial fatigue limit criterion- Theory and application". In: *Biaxial and multiaxial fatigue (A 90-16739 05-39). London, Mechanical Engineering Publications, Ltd.* (1989), pp. 479–496.

[99] Y. Jiang and H. Sehitoglu. "A model for rolling contact failure". en. In: *Wear* 224.1 (Jan. 1999), pp. 38–49. ISSN: 0043-1648. DOI: 10.1016/S0043-1648(98)00311-1.

[100] T. Telliskivi et al. "A tool and a method for FE analysis of wheel and rail interaction". en. In: *Proceedings of the ANSYS 2000 Technical Conference, Pittsburg, US* (2000).

[101] A. Zhu et al. "Research on Prediction of Metro Wheel Wear Based on Integrated Data-Model-Driven Approach". In: *IEEE Access* 7 (2019), pp. 153–166. ISSN: 2169-3536. DOI: 10.1109/ACCESS.2019.2950391.

[102] Y. Ye et al. "Predicting railway wheel wear by calibrating existing wear models: Principle and application". In: *Reliability Engineering & System Safety* 238 (Oct. 2023). 109462. ISSN: 0951-8320. DOI: 10.1016/j.ress.2023.109462.

[103] B. Wen, G. Tao, and Z. Wen. "Prediction of locomotive wheel wear evolution considering thermo-mechanical coupling: Wear model and validation". In: *Wear* (Jan. 2025). 205805. ISSN: 0043-1648. DOI: 10.1016/j.wear.2025.205805.

[104] R. Enblom and M. Berg. "Impact of non-elliptic contact modelling in wheel wear simulation". In: *Wear*. Contact Mechanics and Wear of Rail/Wheel Systems - CM2006 265.9 (Oct. 2008), pp. 1532–1541. ISSN: 0043-1648. DOI: 10.1016/j.wear.2008.01.027.

[105] G. Tao et al. "Effects of wheel–rail contact modelling on wheel wear simulation". In: *Wear*. Contact Mechanics and Wear of Rail / Wheel Systems, CM2015, August 2015 366-367 (Nov. 2016), pp. 146–156. ISSN: 0043-1648. DOI: 10.1016/j.wear.2016.05.010.

[106] A. Olsson, G. Sandberg, and O. Dahlblom. "On Latin hypercube sampling for structural reliability analysis". In: *Structural Safety* 25.1 (Jan. 2003), pp. 47–68. ISSN: 0167-4730. DOI: 10.1016/S0167-4730(02)00039-5.

[107] D. S. Broomhead. "Multivariable Functional Interpolation and Adaptive Networks". en. In: *Complex Systems 2.3* 1988 (), pp. 321–355.

[108] C. E. Rasmussen. "Gaussian Processes in Machine Learning". en. In: *Advanced Lectures on Machine Learning: ML Summer Schools 2003, Canberra, Australia, February 2 - 14, 2003, Tübingen, Germany, August 4 - 16, 2003, Revised Lectures*. Ed. by O. Bousquet, U. von Luxburg, and G. Rätsch. Berlin, Heidelberg: Springer, 2004, pp. 63–71. ISBN: 978-3-540-28650-9. DOI: 10.1007/978-3-540-28650-9_4.

[109] C. L. Pun et al. "An efficient computational approach to evaluate the ratcheting performance of rail steels under cyclic rolling contact in service". In: *International Journal of Mechanical Sciences* 101-102 (Oct. 2015), pp. 214–226. ISSN: 0020-7403. DOI: 10.1016/j.ijmecsci.2015.08.008.

[110] J. Donea. "Arbitrary Lagrangian-Eulerian finite element analysis". In: *Computational methods for Transient Analyasis* (1983), pp. 474–516.

[111] T. J. R. Hughes, W. K. Liu, and T. K. Zimmermann. "Lagrangian-Eulerian finite element formulation for incompressible viscous flows". In: *Computer Methods in*

Applied Mechanics and Engineering 29.3 (Dec. 1981), pp. 329–349. ISSN: 0045-7825. DOI: 10.1016/0045-7825(81)90049-9.

[112] J. Donea et al. "Arbitrary Lagrangian–Eulerian Methods". en. In: *Encyclopedia of Computational Mechanics*. Chichester: Wiley Online Library, 2004. ISBN: 978-0-470-84699-5.

[113] U. Nackenhorst. "On the finite element analysis of steady state rolling contact". In: *Contact Mechanics––Computational Techniques, Computational Mechanics Publication* (1993), pp. 53–60. ISSN: 1743-3533.

[114] U. Nackenhorst. "The ALE-formulation of bodies in rolling contact: Theoretical foundations and finite element approach". In: *Computer Methods in Applied Mechanics and Engineering*. The Arbitrary Lagrangian-Eulerian Formulation 193.39 (Oct. 2004), pp. 4299–4322. ISSN: 0045-7825. DOI: 10.1016/j.cma.2004.01.033.

[115] S. Damme et al. "On the Numerical Analysis of the Wheel-Rail System in Rolling Contact". en. In: *System Dynamics and Long-Term Behaviour of Railway Vehicles, Track and Subgrade*. Ed. by K. Popp and W. Schiehlen. Berlin, Heidelberg: Springer, 2003, pp. 155–174. ISBN: 978-3-540-45476-2. DOI: 10.1007/978-3-540-45476-2_10.

[116] I. Wollny and M. Kaliske. "Numerical simulation of pavement structures with inelastic material behaviour under rolling tyres based on an arbitrary Lagrangian Eulerian (ALE) formulation". In: *Road Materials and Pavement Design* 14.1 (Mar. 2013), pp. 71–89. ISSN: 1468-0629. DOI: 10.1080/14680629.2012.735800.

[117] I. Wollny, F. Hartung, and M. Kaliske. "Numerical modeling of inelastic structures at loading of steady state rolling". en. In: *Computational Mechanics* 57.5 (May 2016), pp. 867–886. ISSN: 1432-0924. DOI: 10.1007/s00466-016-1266-2.

[118] A. Anantheswar, I. Wollny, and M. Kaliske. "A dynamic ALE formulation for structures under moving loads". en. In: *Computational Mechanics* 73.1 (Jan. 2024), pp. 139–157. ISSN: 1432-0924. DOI: 10.1007/s00466-023-02360-5.

[119] A. Anantheswar, I. Wollny, and M. Kaliske. "Treatment of inelastic material models within a dynamic ALE formulation for structures subjected to moving loads". en. In: *International Journal for Numerical Methods in Engineering* 126.1 (2025), e7599. ISSN: 1097-0207. DOI: 10.1002/nme.7599.

[120] W. Shen and D. J. Kirkner. "Non-linear Finite-Element Analysis to Predict Permanent Deformations in Pavement Structures Under Moving Loads". In: *International Journal of Pavement Engineering* 2.3 (Nov. 2001), pp. 187–199. ISSN: 1029-8436. DOI: 10.1080/10298430108901726.

[121] K. Dang Van and M. H. Maitournam. "Steady-state flow in classical elastoplasticity: Applications to repeated rolling and sliding contact". In: *Journal of the Mechanics and Physics of Solids* 41.11 (Nov. 1993), pp. 1691–1710. ISSN: 0022-5096. DOI: 10.1016/0022-5096(93)90027-D.

[122] K. Dang Van, M. Maitournam, and B. Prasil. "Elastoplastic analysis of repeated moving contact application to railways damage phenomena". en. In: *Wear* 196.1-2 (Aug. 1996), pp. 77–81. ISSN: 00431648. DOI: 10.1016/0043-1648(95)06864-3.

[123] K. Dang Van and M. H. Maitournam. "On some recent trends in modelling of contact fatigue and wear in rail". In: *Wear*. CM2000 S.I. 253.1 (July 2002), pp. 219–227. ISSN: 0043-1648. DOI: 10.1016/S0043-1648(02)00104-7.

[124] A. Draganis, F. Larsson, and A. Ekberg. “Numerical evaluation of the transient response due to non-smooth rolling contact using an arbitrary Lagrangian–Eulerian formulation”. en. In: *Proceedings of the Institution of Mechanical Engineers, Part J: Journal of Engineering Tribology* 226.1 (Jan. 2012), pp. 36–45. ISSN: 1350-6501. DOI: 10.1177/1350650111422015.

[125] S. Hazar et al. “Modeling of steady-state crack growth in shape memory alloys using a stationary method”. In: *International Journal of Plasticity* 67 (Apr. 2015), pp. 26–38. ISSN: 0749-6419. DOI: 10.1016/j.ijplas.2014.08.018.

[126] S. Gawade. “The Newton-Raphson Method: A Detailed Analysis”. en. In: *International Journal for Research in Applied Science and Engineering Technology* 12.11 (Nov. 2024), pp. 729–734. ISSN: 23219653. DOI: 10.22214/ijraset.2024.65147.

[127] G. Berkooz, P. Holmes, and J. L. Lumley. “The Proper Orthogonal Decomposition in the Analysis of Turbulent Flows”. In: *Annual Review of Fluid Mechanics* 25.1 (1993), pp. 539–575. DOI: 10.1146/annurev.fl.25.010193.002543.

[128] A. Chatterjee. “An introduction to the proper orthogonal decomposition”. In: *Current Science* 78.7 (2000). Publisher: Temporary Publisher, pp. 808–817. ISSN: 0011-3891.

[129] H. Abdi and L. J. Williams. “Principal component analysis”. en. In: *WIREs Computational Statistics* 2.4 (2010), pp. 433–459. ISSN: 1939-0068. DOI: 10.1002/wics.101.

[130] G. H. Golub and C. Reinsch. “Singular Value Decomposition and Least Squares Solutions”. en. In: *Linear algebra* (1971), pp. 134–151.

[131] V. Klema and A. Laub. “The singular value decomposition: Its computation and some applications”. In: *IEEE Transactions on Automatic Control* 25.2 (Apr. 1980), pp. 164–176. ISSN: 1558-2523. DOI: 10.1109/TAC.1980.1102314.

[132] A. Ammar et al. “A new family of solvers for some classes of multidimensional partial differential equations encountered in kinetic theory modeling of complex fluids”. en. In: *Journal of Non-Newtonian Fluid Mechanics* 139.3 (Dec. 2006), pp. 153–176. ISSN: 0377-0257. DOI: 10.1016/j.jnnfm.2006.07.007.

[133] A. Ammar et al. “A new family of solvers for some classes of multidimensional partial differential equations encountered in kinetic theory modelling of complex fluids: Part II: Transient simulation using space-time separated representations”. en. In: *Journal of Non-Newtonian Fluid Mechanics* 144.2 (July 2007), pp. 98–121. ISSN: 0377-0257. DOI: 10.1016/j.jnnfm.2007.03.009.

[134] A. Ammar et al. “An error estimator for separated representations of highly multidimensional models”. en. In: *Computer Methods in Applied Mechanics and Engineering* 199.25 (May 2010), pp. 1872–1880. ISSN: 0045-7825. DOI: 10.1016/j.cma.2010.02.012.

[135] F. Chinesta, A. Ammar, and E. Cueto. “Recent advances and new challenges in the use of the Proper Generalized Decomposition for solving multidimensional models”. en. In: *Archives of Computational Methods in Engineering* 17.4 (Dec. 2010), pp. 327–350. ISSN: 1886-1784. DOI: 10.1007/s11831-010-9049-y.

[136] A. Ammar, M. Normandin, and F. Chinesta. “Solving parametric complex fluids models in rheometric flows”. en. In: *Journal of Non-Newtonian Fluid Mechanics*

165.23 (Dec. 2010), pp. 1588–1601. ISSN: 0377-0257. DOI: 10.1016/j.jnnfm.2010.08.006.

[137] E. Pruliere, F. Chinesta, and A. Ammar. "On the deterministic solution of multidimensional parametric models using the Proper Generalized Decomposition". en. In: *Mathematics and Computers in Simulation* 81.4 (Dec. 2010), pp. 791–810. ISSN: 0378-4754. DOI: 10.1016/j.matcom.2010.07.015.

[138] E. Giner et al. "The Proper Generalized Decomposition (PGD) as a numerical procedure to solve 3D cracked plates in linear elastic fracture mechanics". en. In: *International Journal of Solids and Structures* 50.10 (May 2013), pp. 1710–1720. ISSN: 0020-7683. DOI: 10.1016/j.ijsolstr.2013.01.039.

[139] X. Zou et al. "A nonintrusive proper generalized decomposition scheme with application in biomechanics". en. In: *International Journal for Numerical Methods in Engineering* 113.2 (2018), pp. 230–251. ISSN: 1097-0207. DOI: 10.1002/nme.5610.

[140] D. González et al. "Recent advances on the use of separated representations". en. In: *International Journal for Numerical Methods in Engineering* 81.5 (2010), pp. 637–659. ISSN: 1097-0207. DOI: 10.1002/nme.2710.

[141] B. Bognet et al. "Advanced simulation of models defined in plate geometries: 3D solutions with 2D computational complexity". en. In: *Computer Methods in Applied Mechanics and Engineering* 201-204 (Jan. 2012), pp. 1–12. ISSN: 0045-7825. DOI: 10.1016/j.cma.2011.08.025.

[142] B. Bognet, A. Leygue, and F. Chinesta. "On the fully 3D simulations of thermoelastic models defined in plate and shell geometries". en. In: *European Journal of Computational Mechanics* 21.1-2 (Apr. 2012), pp. 40–51. ISSN: 1779-7179, 1958-5829. DOI: 10.1080/17797179.2012.702429.

[143] P. Benner et al., eds. *Model Order Reduction: Volume 2: Snapshot-Based Methods and Algorithms*. English. Accepted: 2021-02-11T17:55:54Z. De Gruyter, 2020. DOI: 10.1515/9783110671490.

[144] M. Vitse, D. Néron, and P.-A. Boucard. "Dealing with a nonlinear material behavior and its variability through PGD models: Application to reinforced concrete structures". In: *Finite Elements in Analysis and Design* 153 (Jan. 2019), pp. 22–37. ISSN: 0168-874X. DOI: 10.1016/j.finel.2018.05.006.

[145] D. Néron, P.-A. Boucard, and N. Relun. "Time-space PGD for the rapid solution of 3D nonlinear parametrized problems in the many-query context". en. In: *International Journal for Numerical Methods in Engineering* 103.4 (2015). _eprint: https://onlinelibrary.wiley.com/doi/pdf/10.1002/nme.4893, pp. 275–292. ISSN: 1097-0207. DOI: 10.1002/nme.4893.

[146] P. Ladaveze. "New algorithms: mechanical framework and development". In: *Compte rendu de l'académie des Sci* 300.2 (1985), pp. 41–44.

[147] P. Ladevèze and A. Nouy. "On a multiscale computational strategy with time and space homogenization for structural mechanics". en. In: *Computer Methods in Applied Mechanics and Engineering*. Multiscale Computational Mechanics for Materials and Structures 192.28 (July 2003), pp. 3061–3087. ISSN: 0045-7825. DOI: 10.1016/S0045-7825(03)00341-4.

[148] P. Ladevèze, J. .-. Passieux, and D. Néron. "The LATIN multiscale computational method and the Proper Generalized Decomposition". en. In: *Computer Methods in*

Applied Mechanics and Engineering. Multiscale Models and Mathematical Aspects in Solid and Fluid Mechanics 199.21 (Apr. 2010), pp. 1287–1296. ISSN: 0045-7825. DOI: 10.1016/j.cma.2009.06.023.

[149] P. Ladeveze. *Nonlinear Computational Structural Mechanics: New Approaches and Non-Incremental Methods of Calculation*. en. Springer Science & Business Media, Dec. 2012. ISBN: 978-1-4612-1432-8.

[150] J. F. Archard, W. Hirst, and T. E. Allibone. "The wear of metals under unlubricated conditions". In: *Proceedings of the Royal Society of London. Series A. Mathematical and Physical Sciences* 236.1206 (Jan. 1997). Publisher: Royal Society, pp. 397–410. DOI: 10.1098/rspa.1956.0144.